

Journal Pre-proof



Longitudinal profiling of respiratory and systemic immune responses reveals myeloid cell-driven lung inflammation in severe COVID-19

Peter A. Szabo, Pranay Dogra, Joshua I. Gray, Steven B. Wells, Thomas J. Connors, Stuart P. Weisberg, Izabela Krupska, Rei Matsumoto, Maya M.L. Poon, Emma Idzikowski, Sinead E. Morris, Chloé Pasin, Andrew J. Yates, Amy Ku, Michael Chait, Julia Davis-Porada, Xinzheng V. Guo, Jing Zhou, Matthew Steinle, Sean Mackay, Anjali Saqi, Matthew R. Baldwin, Peter A. Sims, Donna L. Farber

PII: S1074-7613(21)00117-5

DOI: <https://doi.org/10.1016/j.immuni.2021.03.005>

Reference: IMMUNI 4572

To appear in: *Immunity*

Received Date: 12 October 2020

Revised Date: 27 January 2021

Accepted Date: 5 March 2021

Please cite this article as: Szabo, P.A., Dogra, P., Gray, J.I., Wells, S.B., Connors, T.J., Weisberg, S.P., Krupska, I., Matsumoto, R., Poon, M.M.L., Idzikowski, E., Morris, S.E., Pasin, C., Yates, A.J., Ku, A., Chait, M., Davis-Porada, J., Guo, X.V., Zhou, J., Steinle, M., Mackay, S., Saqi, A., Baldwin, M.R., Sims, P.A., Farber, D.L., Longitudinal profiling of respiratory and systemic immune responses reveals myeloid cell-driven lung inflammation in severe COVID-19, *Immunity* (2021), doi: <https://doi.org/10.1016/j.immuni.2021.03.005>.

This is a PDF file of an article that has undergone enhancements after acceptance, such as the addition of a cover page and metadata, and formatting for readability, but it is not yet the definitive version of record. This version will undergo additional copyediting, typesetting and review before it is published in its final form, but we are providing this version to give early visibility of the article. Please note that, during the production process, errors may be discovered which could affect the content, and all legal disclaimers that apply to the journal pertain.

© 2021 Elsevier Inc.

1
2
3
4
5
6
7
8
9
10
11
12
13
14
15
16
17
18
19
20
21
22
23
24
25
26
27
28
29
30
31
32
33
34
35

Longitudinal profiling of respiratory and systemic immune responses reveals myeloid cell-driven lung inflammation in severe COVID-19

Peter A. Szabo^{1,11}, Pranay Dogra^{1,11}, Joshua I. Gray^{1,11}, Steven B. Wells^{2,11}, Thomas J. Connors³, Stuart P. Weisberg⁴, Izabela Krupska², Rei Matsumoto⁵, Maya M.L. Poon^{1,6}, Emma Idzikowski³, Sinead E. Morris⁴, Chloé Pasin⁴, Andrew J. Yates⁴, Amy Ku⁴, Michael Chait⁴, Julia Davis-Porada⁶, Xinzheng V. Guo⁷, Jing Zhou⁸, Matthew Steinle⁸, Sean Mackay⁸, Anjali Saqi⁴, Matthew R. Baldwin⁹, Peter A. Sims^{2,10} and Donna L. Farber^{1,5*}

¹Department of Microbiology and Immunology, Columbia University Irving Medical Center, New York, NY 10032

²Department of Systems Biology, Columbia University Irving Medical Center, New York, NY 10032

³Department of Pediatrics, Columbia University Irving Medical Center, New York, NY 10032

⁴Department of Pathology and Cell Biology, Columbia University Irving Medical Center, New York, NY 10032

⁵Department of Surgery, Columbia University Irving Medical Center, New York, NY 10032

⁶Medical Scientist Training Program, Columbia University

⁷Human Immune Monitoring Core, Columbia University Irving Medical Center, New York, NY 10032

⁸IsoPlexis Corporation, Branford, CT 06405

⁹Department of Medicine, Columbia University Irving Medical Center, New York, NY 10032

¹⁰Department of Biochemistry and Molecular Biophysics, Columbia University Irving Medical Center, New York, NY 10032

¹¹These authors contributed equally

¹²Lead Contact

*Correspondence: df2396@cumc.columbia.edu

1 SUMMARY

2 Immune response dynamics in COVID-19 and its severe manifestations have largely
3 been studied in circulation. Here, we examined the relationship between immune processes in the
4 respiratory tract and circulation through longitudinal phenotypic, transcriptomic and cytokine
5 profiling of paired airway and blood samples from patients with severe COVID-19 relative to
6 healthy controls. In COVID-19 airways, T cells exhibited activated, tissue-resident, and
7 protective profiles; higher T cell frequencies correlated with survival and younger age. Myeloid
8 cells in COVID-19 airways featured hyper-inflammatory signatures and higher frequencies of
9 these cells correlated with mortality and older age. In COVID-19 blood, aberrant CD163⁺
10 monocytes predominated over conventional monocytes, and were found in corresponding airway
11 samples and in damaged alveoli. High levels of myeloid chemoattractants in airways suggest
12 recruitment of these cells through a CCL2-CCR2 chemokine axis. Our findings provide insights
13 into immune processes driving COVID-19 lung pathology with therapeutic implications for
14 targeting inflammation in the respiratory tract.

15

16 **Key Words:** COVID-19, lung immunity, ARDS, tissue resident memory T cells, macrophages

17

1 INTRODUCTION

2 The respiratory virus SARS-CoV-2 has resulted in devastating impacts to the world's
3 population due to morbidity and mortality of COVID-19, as well as the life-altering measures
4 implemented to mitigate spread. While the majority of infected individuals (>90%) develop a
5 self-limiting disease and recover, approximately 5-10% of individuals develop severe respiratory
6 disease marked by lung infiltrates and reduced oxygen saturation, which can progress to acute
7 respiratory distress syndrome (ARDS), multi-organ failure, and death (Wu and McGoogan,
8 2020). To date, well over 2 million individuals have succumbed to COVID-19 including
9 >500,000 in the US alone. Risk factors for severe COVID-19 include older age and co-
10 morbidities such as obesity, diabetes, and hypertension, although younger and previously healthy
11 individuals are also susceptible (Cummings et al., 2020; Davies et al., 2020). For individuals
12 who recover from self-limiting illness, the immune system acts in a coordinated fashion to clear
13 the virus and establish virus-specific immunity (Rydzynski Moderbacher et al., 2020). However,
14 the role of the immune response in the pathogenesis of severe COVID-19 remains unclear and
15 understanding this phenomenon is urgently required to develop new treatment and prevention
16 strategies.

17 Immune responses to respiratory virus infection are focused in the lung, where innate
18 immune responses are initiated by tissue-resident alveolar macrophages as well as infiltrating
19 monocytes and granulocytes (Yoo et al., 2013). The initial production of pro-inflammatory
20 cytokines in the lung can precipitate cytokine storms in severe respiratory infections (Teijaro et
21 al., 2011b). Adaptive immune responses mediated by CD4⁺ and CD8⁺ T cells involve
22 mobilization of effector T cells to the lung for mediating clearance of infected cells *in situ*
23 (Kohlmeier and Woodland, 2009). A proportion of these lung effector T cells develop into

1 tissue-resident memory T cells (TRM), which are retained in the lung and can mediate rapid
2 protective responses upon viral challenge (Teijaro et al., 2011a; Turner et al., 2014; Turner and
3 Farber, 2014; Wu et al., 2014). In mouse models of SARS-CoV-1 infection, CD4⁺ TRM-like
4 cells in the airway are required for protection (Zhao et al., 2016). In adult lungs, TRM are the
5 predominant T cell subset and persist in stable frequencies throughout many decades of life
6 (Kumar et al., 2018; Thome et al., 2014), suggesting a crucial role in protection to respiratory
7 pathogens. The role of resident immune cells, including alveolar macrophages and lung TRM in
8 protection against SARS-CoV-2 infection, and their function in the pathogenesis of severe
9 COVID-19 have yet to be elucidated.

10 Studies of the immune response to SARS-CoV-2 have examined innate and adaptive
11 immune cells as well as soluble mediators in circulation of infected individuals, revealing
12 elevated pro-inflammatory cytokines (Hadjadj et al., 2020; Laing et al., 2020) and alterations in
13 immune cell composition (Lucas et al., 2020; Mathew et al., 2020). Robust virus-specific
14 adaptive immune responses have also been identified in blood of individuals during acute
15 infection and following recovery, including virus-specific CD4⁺ and CD8⁺ T cells (Grifoni et al.,
16 2020; Thieme et al., 2020; Weiskopf et al., 2020), and neutralizing antibodies specific for viral
17 proteins (Long et al., 2020; Ni et al., 2020). How these systemic immune responses relate to
18 innate and adaptive immunity in the respiratory tract and their contribution to disease is unclear
19 and difficult to assess.

20 Here, we sought to define the dynamic immune processes involved in pathogenesis of
21 severe COVID-19 by high-dimensional phenotypic, transcriptomic, and functional profiling of
22 immune responses in paired airway and blood samples obtained longitudinally from patients with
23 severe COVID-19. This analysis, in conjunction with airway and blood samples from uninfected

1 controls, suggests key functional roles for airway T cells and monocyte/macrophages associated
2 with disease outcome. T cells in COVID-19 airways exhibited activated and tissue-resident
3 signatures, functionally protective signatures, and their frequencies in airways (but not in blood)
4 correlated with younger age and survival. Conversely, airway myeloid cells exhibited hyper-
5 inflammatory signatures producing chemokines such as CCL2 and CCL3, while the blood
6 contained aberrant CD163^{hi} and HLA-DR^{lo} monocyte populations expressing the chemokine
7 receptor CCR2. Accordingly, infiltrating airway myeloid cells in severe COVID-19 airways
8 likely derive from recruitment from circulation, and their frequency was associated with older
9 age and mortality. Our results provide evidence for myeloid cell-driven lung inflammation in
10 severe COVID-19 and reveal potential targets for reducing lung damage by inhibiting airway-
11 specific inflammatory processes.

12

1 RESULTS

2 **Obtaining paired airway and blood samples from severe COVID-19 patients and controls**

3 During the height of the pandemic in New York City, between April and June 2020, we
4 enrolled patients from adult and pediatric intensive care units at New York Presbyterian hospital
5 with severe COVID-19 (see methods for enrollment criteria). All enrolled patients exhibited
6 clinical features of ARDS requiring mechanical ventilator support and intubation. We obtained
7 daily paired airway and blood samples longitudinally from these patients starting at 24-36 hours
8 after intubation, and continuing for up to 10 days during their hospitalization (average 6-7
9 sample days per patient; sample numbers varied due to patient extubation or death during
10 enrollment). Patients represented a broad age range (14-84 years old) and 8/15 (53%) died during
11 enrollment or soon after (Table S1). Enrolled COVID-19 patients exhibited similar clinical
12 features of disease severity and ARDS independent of outcome as assessed by markers of
13 inflammation, neutrophil levels, Sequential Organ Failure Assessment (SOFA) score (Jones et
14 al., 2009), and PaO₂/FiO₂ (P/F) ratios (Ranieri et al., 2012). Comorbidities were similar between
15 deceased patients and those who survived, while the median age of survivors was significantly
16 younger than those who succumbed (39 versus 72 years old). Treatments including steroids, anti-
17 IL-6 therapy, and Remdesivir were given comparably to both groups and were not associated
18 with mortality (Table S1). All patients developed robust SARS-CoV-2-specific neutralizing
19 antibodies as measured in plasma (Weisberg et al., 2021).

20 Airway samples were obtained using a saline wash of the endotracheal tube performed
21 daily as part of clinical care, which we have previously shown contains respiratory immune cell
22 populations (Connors et al., 2018; Connors et al., 2016). A total of 141 blood and airway cell
23 preparations from COVID-19 patients were analyzed by high-dimensional spectral flow

1 cytometry in comparison to airway samples obtained from washes of healthy control lungs
2 (Snyder et al., 2019) and blood samples from healthy volunteers (n=5, see methods). Airway
3 supernatants and blood plasma at early and late timepoints were assayed for cytokine and
4 chemokine protein content and successive samples from four COVID-19 patients were profiled
5 by scRNA-seq (Figure 1A, Table S2, S3).

6

7 **Distinct immune cell composition in the airway and blood of severe COVID-19 patients**

8 Mononuclear cells in airway and blood samples were isolated from severe COVID-19
9 patients and uninfected healthy controls (see methods), stained using a 34 marker panel
10 containing antibodies specific for major lineage determinants and markers for differentiation,
11 tissue residence, activation, and function (see Key Resources Table), and analyzed by spectral
12 flow cytometry (gating strategy for mononuclear cells shown in Figure S1). Principal component
13 analysis (PCA) of mean marker expression for each sample segregated airway and blood samples
14 along PC2, but not by individual (Figure 1B). While healthy airway samples intermixed with
15 COVID-19 airway samples, healthy blood segregated from COVID-19 blood samples along PC1
16 (Figure 1B, Table S4). Uniform manifold approximation and projection (UMAP) embeddings of
17 flow cytometry data from all COVID-19 and control samples showed distinct separation of the
18 major lineages into myeloid cells, CD4⁺ T cells, CD8⁺ T cells, B cells, and innate lymphoid cells
19 (ILCs) that were predominantly NK cells (Figure 1C, Figure S1B).

20 Quantitative comparison of immune cell frequencies between severe COVID-19 and
21 healthy samples for each site revealed disease and site-associated variations. Airways exhibited
22 similar immune cell composition between COVID-19 and controls, with predominant myeloid
23 cells, lower frequencies of T cells, and negligible B cells and ILCs. By contrast, blood samples

1 had multiple differences in immune cells composition between COVID-19 and controls,
2 including decreases in CD4⁺ and CD8⁺ T cell frequencies, and substantial increases in myeloid
3 cell frequencies (Figure 1D), consistent with previous studies (Lucas et al., 2020). Our
4 longitudinal sampling from COVID-19 patients demonstrated that the distinct immune cell
5 compositions in airway and blood were stable across time (Figure 1E). These findings indicate
6 compartmentalized distribution of immune cells in the airways during homeostasis and severe
7 COVID-19, along with disease-driven changes in overall immune cell composition more highly
8 manifested in blood.

10 **Age-related alterations in airway immune cell subsets are associated with survival from** 11 **severe COVID-19**

12 Age is a strong independent risk factor for death in COVID-19 (Cummings et al., 2020;
13 Garibaldi et al., 2021). We investigated whether the overall immune cell composition in airways
14 and blood (average of all longitudinal samples obtained for each patient) was altered with age
15 and/or associated with patient outcome. There were statistically significant correlations of age
16 with immune cell frequencies in airways but not with those in blood (Figure 2A, Figure S2A). In
17 particular, there was a strong positive correlation of airway myeloid cells with age (Spearman's
18 $\rho = 0.65$), while airway total and CD4⁺T cell frequencies were inversely correlated with age
19 (Spearman's $\rho = -0.56$ and -0.69 , respectively) (Figure 2A). Notably, mortality from severe
20 COVID-19 was exclusive to older patients in the cohort (Figure 2A).

21 Our acquisition of longitudinal data enabled assessment of immune cell and clinical
22 trajectories for their potential associations with disease outcome. Using an area under the curve
23 (AUC) calculation, we found differences in the immune cell frequencies of both airway T cells

1 and myeloid cells as well as blood myeloid cells of patients who died versus those who survived
2 (Figure 2B). The frequencies of other immune cells in airway (B cells, ILC) and blood (T cells,
3 B cells, and ILCs) did not differ between these groups (Figure 2B, Figure S2A). We further
4 investigated whether the longitudinal trajectories of immune cell composition in the airway or
5 blood were predictive of outcome, relative to corresponding clinical measurements of disease
6 severity (SOFA scores and P/F ratio). We used a k-means clustering approach (see methods) to
7 classify the temporal dynamics of immune cell frequencies and clinical measurements (Figure
8 2C). The clinical parameters (SOFA score and P/F ratio) and immune cell frequencies in the
9 blood did not predict outcome (~50% success rate), whereas both T and myeloid cell frequencies
10 in the airway were predictive of outcome with a 75% success rate (Figure 2C). Together, these
11 results show that frequencies of T and myeloid cells in the airways were associated with age and
12 outcome, suggesting specific roles for these cell populations in COVID-19 disease pathogenesis.
13

14 **Tissue-resident memory T cells predominate in airways and become activated in severe** 15 **COVID-19**

16 The subset composition of airway and blood T cells in severe COVID-19 versus healthy
17 controls was examined using computational analysis of the high dimensional flow cytometry
18 data. Multiple markers of T cell differentiation were used to distinguish CD4⁺ and CD8⁺ naïve
19 (CD45RA⁺CCR7⁺) and memory subsets (CD45RA⁻CCR7^{-/+}CD95⁺), TRM (CD69⁺CD103^{+/-}),
20 regulatory T cells (Tregs; CD4⁺CD25⁺CD127⁻Foxp3⁺), along with markers of activation (HLA-
21 DR, PD-1), co-stimulation (CD27, CD28), senescence and terminal differentiation (CD57,
22 KLRG1), and $\gamma\delta$ T cells (TCR $\gamma\delta$) (Figure 3A). We used UMAP embeddings to visualize
23 expression of these multiple markers by the combined airway and blood T cell dataset, showing

1 segregation of the CD4⁺ lineage on the left, CD8⁺ on the right, and airway T cells segregating at
2 the top of each embedding (Figure S3A). There was biased expression of CD69, CD103, PD-1,
3 and HLA-DR in the airways while CCR7, CD45RA, and CD127 expression was more prevalent
4 in the blood (Figure S3A).

5 To analyze specific subsets of T cells, Phenograph clustering based on marker expression
6 yielded 24 clusters, which were coalesced into 13 denoting biological subsets, functional, and/or
7 activation states in the airway and blood (Figure 3A). Compositional analysis shown by UMAP
8 embeddings, corresponding pie charts depicting frequency of each subset in the aggregated data
9 (Figure 3B), and quantification of individual compiled and paired data (Figure 3C, S3B),
10 demonstrated site- and disease-associated alterations in T cell subsets induced by severe COVID-
11 19. T cells in COVID-19 airways were predominantly CD4⁺ and CD8⁺ TRM, as in healthy
12 airways, and showed elevated proportions of activated TRM and TEM subsets expressing HLA-
13 DR, PD-1, and reduced levels of CD127 (Figure 3A-C). Severe COVID-19 airways also
14 contained reduced Treg frequencies compared to healthy airways (Figure 3B, C) and overall
15 increased frequencies of circulating TEM and TCM cells in the aggregated analysis (Figure 3B).
16 Together, these results suggest that T cells are being activated *in situ* as well as recruited to the
17 respiratory tract.

18 By contrast, T cell subset proportions in the COVID-19 blood were similar to that of
19 healthy controls, with comparable frequencies of naïve, TCM and TEM populations for both
20 CD4⁺ and CD8⁺ lineages, though some COVID-19 patients showed an increase in blood CD4⁺
21 TEM cells (Figure 3B, C). Both COVID-19 and healthy blood lacked measurable TRM cells
22 which were compartmentalized exclusively in the airways, consistent with previous studies
23 showing TRM in airway and lungs but not blood during homeostasis (Kumar et al., 2017;

1 Sathaliyawala et al., 2013; Snyder et al., 2019; Thome et al., 2014). Importantly, activation
2 markers (HLA-DR, PD-1) were highly expressed by T cells specifically in COVID-19 airways,
3 compared to the low level of expression by T cells in COVID-19 blood and in both control sites
4 (Figure 3D). Together, these analyses indicate that activated T cells responding to the ongoing
5 infection in severe COVID-19 were localized to the airways and are not present at high levels in
6 circulation – a finding consistent with airway, but not blood T cells associated with improved
7 outcome.

8

9 **Dysregulation of myeloid cells in the airways and blood of severe COVID-19**

10 We applied similar high-dimensional analysis to identify subsets of myeloid populations
11 in aggregated airway and blood samples from severe COVID-19 patients and healthy controls.
12 Phenograph clustering of myeloid marker expression identified 21 clusters, which were
13 coalesced into 9 clusters based on phenotypic similarity to classical and intermediate monocyte
14 subsets (based on CD14 and CD16 expression) (Kapellos et al., 2019), macrophage subsets
15 based on CD163 expression (Bharat et al., 2016), along with key differentially expressed
16 markers HLA-DR, CD86, and CD11c (Figure 4A, Figure S4A). Data were visualized by UMAP
17 and pie charts (Figure 4B) as with T cells in Figure 3.

18 Severe COVID-19 airways and blood showed profound and significant alterations in the
19 compartmentalization, distribution and phenotypes of myeloid cell subsets compared to healthy
20 controls (Figure 4B, C). In healthy controls, the myeloid populations in airway and blood were
21 distinct; airway predominately contained CD163^{hi} macrophages, with a minor CD163^{lo} subset, as
22 well as monocyte populations (CD163^{hi} and intermediate subset) not found in blood (Figure 4B,
23 C). Healthy blood contained a preponderance of HLA-DR^{hi} classical monocytes (typically

1 ~80%) with dendritic cells (DCs) comprising the remaining myeloid cells (Figure 4B, C). By
2 contrast, COVID-19 airway exhibited substantial phenotypic overlap with blood myeloid
3 subsets, suggesting infiltration from blood to airway. In COVID-19 airways, conventional
4 CD163^{hi} macrophages (blue) were present along with an increased frequency of CD163^{lo}HLA-
5 DR^{lo} (green) and CD86^{hi}HLA-DR^{hi} cells (yellow) relative to control airways, as well as different
6 monocyte subsets also seen in blood (Figure 4B, C). In COVID-19 blood, there were stark
7 differences in monocyte phenotypes including a predominance of CD163^{hi} and HLA-DR^{lo}
8 monocytes that are not significantly present in healthy blood, and additional monocytic subsets
9 that were shared between COVID-19 airway and blood (Figure 4B, C). This analysis showed
10 major aberrations in the distribution, phenotype and composition of myeloid cells in the airway
11 and blood of severe COVID-19 patients.

12 To further investigate COVID-19-associated features of myeloid cells for each site, we
13 analyzed coordinate expression of antigen-presentation related molecules HLA-DR and CD86,
14 functional myeloid markers CD64 and CD163, and CD14 and CD16 expression, which define
15 monocyte subsets (Geissmann et al., 2003). While HLA-DR remained highly expressed among
16 myeloid cells in COVID-19 airways, myeloid cells in the blood showed a profound reduction of
17 HLA-DR expression relative healthy controls, reflecting recent findings and suggesting a
18 dysregulated or immature phenotype (Figure 4D) (Schulte-Schrepping et al., 2020). Conversely,
19 airway myeloid cells in COVID-19 patients exhibited CD163 expression similar to levels
20 expressed by CD163^{hi}HLA-DR^{lo} monocytes aberrantly present in blood, which was at a lower
21 level compared to healthy airway CD163^{hi} macrophages (Figure 4E). Lastly, COVID-19 airways
22 exhibited a striking reduction of CD16-expressing monocytes denoting an intermediate
23 phenotype (CD14⁺CD16⁺) compared to healthy controls (Figure 4F). Moreover, all COVID-19

1 blood monocyte subsets showed a reduction of HLA-DR^{hi} cells relative to their respective
2 healthy controls (Figure S4B). Taken together, our results indicate dysregulated monocytes in the
3 blood, alterations of airway macrophages, and evidence for infiltration of aberrant monocyte
4 populations into the airways—a finding consistent with increased airway myeloid cells
5 associated with worse outcome.

6

7 **Single cell transcriptome profiling reveals biased expression of activated and inflammatory** 8 **signatures in airway immune cells**

9 To dissect the functional states of T and myeloid cells in severe COVID-19, we applied
10 transcriptome profiling by scRNA-seq to daily paired airway and blood samples from 4 patients
11 (total of 126,564 cells, Table S3). This scRNA-seq profiling identified immune cell
12 compositions consistent with flow cytometry results, along with additional airway cell types such
13 as epithelial cells and ionocytes (Figures S5A, B, Figure S6A, B). We performed coordinate
14 analysis of the transcriptomic profile of T and myeloid cells between airways and blood to
15 identify how the immune processes in the respiratory tract were connected to those in circulation.

16 For T cells, scRNA-seq revealed distinct transcriptional profiles expressed by airway
17 compared to circulating T cells, as depicted in UMAP of the aggregated data, and heat maps of
18 differentially expressed genes stratified by individual sample (Figure 5A, B). TRM signature
19 genes *CXCR6* and *ITGAI* were uniquely expressed by airway T cells (Figure 5A, Table S5),
20 consistent with our previous scRNA-seq analysis of human TRM cells in airways and lungs
21 (Snyder et al., 2019; Szabo et al., 2019). Naïve and TCM cells distinguished by *SELL* expression
22 were highly enriched in blood, while *CCL5* expression indicating TEM cells were found in both
23 sites (Figure 5A). The top differentially expressed genes between airway and blood revealed that

1 T cells from the airway exhibited a gene signature associated with TRM and tissue T cells
2 (Kumar et al., 2017; Szabo et al., 2019), including upregulated expression of *CXCR6*, *ITGAI*,
3 *PDCD1*, *LGALS*, *LAG3*, and *RBPJ* compared to blood T cells (Figure 5B, Table S5).
4 Importantly, airway T cells also showed upregulated expression of multiple genes encoding key
5 cytokines and chemokines, including *IFNG*, *CCL2*, and *CCL4* compared to those in blood
6 (Figure 5B), consistent with an activated and pro-inflammatory state. By contrast, blood T cells
7 exhibited higher expression of genes associated with quiescence (*TCF7*, *LEF1*) (Choi et al.,
8 2015) and lymphoid homing (*SELL*) (Figure 5B). These results demonstrated
9 compartmentalization of functionally activated TRM populations exhibiting signatures of
10 protective T cells in the respiratory tract of severe COVID-19. These findings are further
11 consistent with increased T cells in the airways correlating to better outcome.

12 Transcriptome analysis of myeloid cells revealed overlapping lineage markers between
13 airway and blood, yet elevated expression of inflammatory gene signatures in the airway that
14 were consistent across individuals (Figure 5, Table S6). There was similar expression of lineage-
15 defining genes (*CD14*, *FCGR3A*, *CD68*, *CD163*) by myeloid cells in airway and blood (Figure
16 5C, D). Expression of tissue macrophage markers *MARCO* and *MRC1* (CD206) (Bharat et al.,
17 2016) and the integrin *ITGAV* (vitronectin receptor) were specific to airway myeloid cells, while
18 blood myeloid cells expressed transcripts for chemokine and homing/egress receptors (*CX3CR1*,
19 *CCR2*, *SELL*, *SIPR4*) (Figure 5C,D). For genes associated with myeloid cell function, airway
20 myeloid cells exhibited elevated levels of transcripts for multiple inflammatory mediators
21 including chemokines for recruitment of monocyte/macrophages (*CCL2*, *CCL3*, *CCL4*),
22 lymphocytes (*CCL18*, *CCL20*, *CCL23*), and neutrophils (*CXCL3*, *CXCL5*), complement
23 components (*C3*, *CIQB*, *CIQC*), and matrix metalloproteinases (*MMP9*, *MMP14*) implicated in

1 tissue damage in ARDS (Hendrix and Kheradmand, 2017) (Figure 5D). Together, these results
2 demonstrate that airway myeloid cells exhibit a hyper-inflammatory state, in the expression of
3 multiple cytokines and chemokines for recruitment of immune cells. In particular, airway-
4 specific expression of CCL2 transcripts along with biased expression of its receptor CCR2 by
5 blood monocytes reveals a potential mechanism for the observed infiltration of blood-derived
6 monocytes into the airway in severe COVID-19.

7 Interferon (IFN)-regulated genes are associated with innate anti-viral immunity and may
8 be dysregulated in COVID-19 (Hadjadj et al., 2020). However, there was negligible expression
9 of genes encoding Type I, Type II, and Type III IFNs from myeloid cells, epithelial cells, or T
10 cells (Figure S6B), consistent with the lack of SARS-CoV-2 viral sequences (see methods) in
11 scRNA-seq data from 4 patients. However, transcripts associated with multiple interferon-
12 regulated gene families (i.e., ISG, IFI, IFIT, IRF, MX and OAS) were detected in both the
13 airway and blood myeloid cells, as well as airway epithelial and T cells (Figure S6B), suggesting
14 a persisting anti-viral state in immune cells across compartments. While expression of IFN-
15 regulated genes may also be triggered by *IFNG* expressed by airway T cells (Figure 5A, B), our
16 scRNA-seq analysis indicates major inflammatory pathways are propagated by airway myeloid
17 cells and may include high level production of chemokines and cytokines for cellular recruitment
18 and promoting tissue damage *in situ*.

19

20 **Inflammatory mediators are highly elevated in the airways during severe COVID-19**

21 To investigate whether the transcript expression of inflammatory markers correlated to
22 secreted proteins, we measured cytokine and chemokine levels in airway supernatants and
23 plasma samples from each COVID-19 patient (Table S2), using a microfluidic multiplexed

1 secretome proteomic platform (Farhadian et al., 2020). Overall, we found marked differences in
2 cytokine and chemokine content in the airway compared to plasma as seen in paired samples and
3 at early (day 1) and later (day 3-7) time points (Figure 6A, Figure S7A, B). Analytes elevated in
4 airways compared to blood include monocyte/macrophage chemoattractants MCP-1 (CCL2),
5 MIP-1 α (CCL3), and MIP1 β (CCL4), and T cell-associated cytokines granzyme B, IL-7, and
6 TNF- β (Figure 6A, 6B, Figure S7B). By contrast, in the blood CCL2 (MCP-1), CCL3 (MIP-1 α),
7 granzyme B, TNF- β , and IL-7 were undetectable, while CCL4 (MIP-1 β) was present at variable
8 levels across patients (Figure 6A, B). Both blood and airways contained low and/or variable
9 levels of molecules associated with T cell effector function (perforin, IFN- γ , IL-17, and IL-2),
10 additional innate cytokines (IL-6 and IL-8), and TGF- β (Figure 6A, B, Figure S7B). Together,
11 these results show the production of pro-inflammatory chemokines and cytokines in the airway
12 with only a subset of these detected in blood.

13 To define the cellular origin of the soluble mediators detected in each compartment, we
14 analyzed transcript expression for each of the molecules in Figure 6B by scRNA-seq. Overall,
15 transcript expression of prominent cytokines/chemokines largely correlated to the protein data;
16 airway myeloid cells expressed high levels of *CCL2*, *CCL3* and *CCL4* transcripts corresponding
17 to the high levels of the respective proteins in airways, while blood myeloid cells expressed
18 lower or undetectable levels of these transcripts (Figure 6C). Airway and blood myeloid cells
19 also expressed *CXCL8* and *TGFBI*, consistent with the protein data (Figure 6C). In the airways,
20 T cells expressed *GZMB*, *CXCL8*, *CCL4*, *PRF*, *IFNG*, and *TGFBI* transcripts, which were
21 expressed by blood T cells at lower or variable levels (Figure 6C). Airway epithelial cells
22 expressed predominantly *CXCL8* transcripts, as well as lower levels of transcripts for IL-7 and
23 several chemokines (Figure 6C). Overall, these results demonstrate a highly inflammatory

1 environment in the airways of severe COVID-19 patients and establish a chemokine gradient for
2 recruiting immune cells from circulation to the site of infection—particularly for the monocyte
3 chemoattractants CCL2 and CCL3.

4

5 **Accumulation of monocytes/macrophages in the lungs of severe COVID-19 patients**

6 We hypothesized that the production of monocyte chemoattractants in the airway may
7 recruit dysregulated blood monocytes into the lung. We therefore examined T and myeloid cells
8 in lung autopsy samples from COVID-19 patients with diffuse alveolar damage, the main
9 pathological finding in COVID-19 ARDS (De Michele et al., 2020), relative to lungs from
10 uninfected organ donor controls (Carpenter et al., 2018) (Table S7). In uninfected lungs, CD4⁺
11 and CD8⁺ T cells were clustered around the airway epithelium, while CD163⁺
12 monocytes/macrophages and neutrophils (MMP9⁺) were dispersed in the parenchyma (Figure
13 7A, top left). In COVID-19 lungs, there was a marked increase in CD163⁺ myeloid cells
14 aggregated in the alveolar spaces, critical sites for oxygenation. Also detectable were CD8⁺ T
15 cells producing granzyme B, consistent with a cytotoxic response (Figure 7A). Quantitative
16 analysis of the lung imaging data showed significant increases in the frequency and density of
17 CD163⁺ myeloid cells in COVID-19 versus uninfected lungs, while numbers and density of
18 lymphocytes (CD4⁺ T cells, CD8⁺ T cells and B cells) and neutrophils were similar between
19 COVID-19 and control lungs (Figure 7B). However, myeloid cells in COVID-19 airway and
20 blood did not express genes associated with proliferation (*Ki67*, *TOP2A*, *UBE2C*) (Figure 7C).
21 These findings together with our phenotypic, transcriptomic and functional analysis of myeloid
22 cells in airway and blood (Figures 4-6), strongly implicate myeloid cell recruitment as a major
23 mechanism perpetuating inflammation and pathogenesis of severe COVID-19.

1 DISCUSSION

2 During the SARS-CoV-2 pandemic, restoration of normal life is impeded first and
3 foremost by the most severe COVID-19 cases, including debilitating ARDS and its high
4 mortality. For respiratory viruses, protective immune responses as well as immunopathology
5 occur in the lung and respiratory tract. While numerous studies demonstrate characteristic
6 features of innate and adaptive immunity to SARS-CoV-2 infection that are detectable in blood
7 (Kuri-Cervantes et al., 2020; Lucas et al., 2020; Mathew et al., 2020; Rydyznski Moderbacher et
8 al., 2020; Schulte-Schrepping et al., 2020), the role of these COVID-19-specific immune
9 alterations in disease pathogenesis is unclear. Several studies have assessed cellular composition
10 within the respiratory environment in bronchoalveolar lavage samples and lung autopsies (Chua
11 et al., 2020; Damiani et al., 2021; Liao et al., 2020; Veras et al., 2020). However, an
12 understanding of the dynamic immune processes in the respiratory tract in the context of
13 circulating immune cell populations is required to dissect mechanisms of disease pathogenesis.

14 In this study, we obtained paired respiratory and blood samples from patients with severe
15 COVID-19 longitudinally during the course of intensive care hospitalization. We employed high
16 dimensional profiling by spectral flow cytometry and scRNA-seq, along with multiplex cytokine
17 quantification and immunofluorescence imaging to characterize airway and systemic immune
18 responses in COVID-19 compared to healthy control samples. Our results suggest functional
19 protective signatures for T cells in the respiratory tract, consistent with their associations with
20 younger age and survival from severe COVID-19. Conversely, we identify a key role for airway
21 myeloid cells, primarily macrophages and monocytes, in driving and perpetuating immune cell
22 recruitment and lung inflammation, consistent with their associations with older age and
23 mortality. We further identify a potential role for CCL2 in promoting recruitment of dysregulated

1 monocytes through a chemotactic axis that could serve as a therapeutic target for reducing lung
2 inflammation and damage in severe COVID-19.

3 A striking feature of T cells in COVID-19 was their biased activation and functional
4 profiles in airways. T cells in COVID-19 airways were predominantly tissue-resident, bearing
5 TRM phenotypes and gene expression profiles similar to control airway. TRM in COVID-19
6 airways exhibited activation profiles, including surface phenotypes (HLA-DR^{hi}PD-1^{hi}CD127^{lo})
7 and upregulated expression of transcripts for effector molecules such as perforin, *GZMB* and
8 *IFNG*—features of protective T cell responses in viral infections. The presence of activated TRM
9 in airways of COVID-19 patients and not in control airways further indicates a virus-directed
10 response. In mouse influenza infection, the presence of activated lung TRM *in situ* to influenza
11 infection correlates with virus-specific responses (Paik and Farber, 2021; Turner et al., 2014),
12 further supporting that *in situ* activation is a surrogate for anti-viral protective responses. Our
13 results also suggest that T cell activation as assessed in circulation during active COVID-19
14 (Mathew et al., 2020; Takahashi et al., 2020) may not reflect T cell responses in the respiratory
15 tract.

16 Myeloid cells in the airways and blood of COVID-19 patients exhibited profound
17 alterations in phenotype, function and compartmentalization. Notably, COVID-19 airways
18 contained tissue macrophages with inflammatory signatures expressing multiple genes encoding
19 pro-inflammatory mediators such as CCL2, CCL3, CCL4, CXCL8, MMP, and complement
20 components. Excessive levels of CCL2 (MCP-1), CCL3 (MIP-1 α), and CCL4 (MIP-1 β) proteins
21 were detected in the airways, but not in blood, further supporting a role of airway myeloid cells
22 in perpetuating inflammatory responses in severe COVID-19. This phenotypic and functional
23 profile of COVID-19 airway monocytes/macrophages shares features with human macrophages

1 in ARDS due to non-infectious causes, including the production of CCL2 and CXCL8, as well as
2 induction of MMPs and complement (Aggarwal et al., 2014; Morrell et al., 2019). Our results
3 indicate that COVID-ARDS shares some key features with ARDS resulting from other infectious
4 or non-infectious causes.

5 Our coordinate analysis of airway and blood myeloid cells and soluble mediators suggest
6 an analogous role for airway macrophages driving lung damage in COVID-19 ARDS through
7 recruitment of circulating monocytes. We show that blood monocytes in severe COVID-19
8 express increased levels of CCR2 transcripts and aberrant CD163^{hi}HLA-DR^{lo}/CD86^{lo}
9 phenotypes compared to healthy blood monocytes. Reduced HLA-DR expression indicative of
10 immature or dysregulated monocytes has been identified in blood myeloid cells in severe
11 COVID-19 (Schulte-Schrepping et al., 2020; Silvin et al., 2020), and may derive from
12 inflammation-induced mobilization from the bone marrow, termed emergency myelopoiesis
13 (Schultze et al., 2019; Shi et al., 2011; Venet et al., 2020). We show that monocyte
14 chemoattractants (CCL2, CCL3) are specifically produced in the respiratory tract, while blood
15 monocytes express the cognate receptor CCR2, suggesting recruitment along a CCL2 gradient as
16 found in ARDS models (Aggarwal et al., 2014). Immunofluorescence imaging of lungs from
17 severe COVID-19 patients also show a striking accumulation of CD163-expressing
18 monocytes/macrophages in the alveolar spaces of the lungs, a key site for blood gas exchange,
19 suggesting their involvement in diffuse alveolar damage observed in COVID-19 pathology (De
20 Michele et al., 2020). Our findings are further consistent with studies of influenza-infected
21 individuals that identified inflammatory monocytes in severe disease (Cole et al., 2017), and
22 increased inflammatory chemokines in the airways, which correlated with airway monocyte
23 infiltration and disease severity (Oshansky et al., 2014).

1 Our results defining airway immune responses in COVID-19 and their relation to the
2 corresponding immune reactants in blood have profound implications for treating and preventing
3 disease. Treatments targeting systemic inflammation, either globally with steroids or specifically
4 with cytokine blockade, have shown variable efficacy in severe COVID-19 (Della-Torre et al.,
5 2020; Furlow, 2020). Our results suggest that targeting airway-derived cytokines such as CCL2
6 through CCR2 antagonists or other airway-specific mediators may be more effective in reducing
7 lung damage or even promoting recovery from ARDS in severe COVID-19. Importantly,
8 preventing CCL2-mediated monocyte recruitment to the lungs was an effective strategy to
9 reduce severity in mouse models of influenza infection (Lin et al., 2008; Lin et al., 2011),
10 suggesting a generalized mechanism for respiratory virus-induced lung injury.

11 Conversely, Airway T cells exhibit protective functional signatures and increased
12 proportions are associated with younger age and survival. Interestingly, monitoring airway T cell
13 frequencies was a more robust predictor of outcome than the SOFA score and P/F ratio, which
14 are two of the most commonly used severity-of-illness measures and strongest predictors of
15 mortality in ARDS (Ranieri et al., 2012; Vincent et al., 1998). While these results require
16 validation in larger cohort studies, airway T cell measurements could be a potentially useful
17 biomarker to monitor patients. In addition, promoting lung-localized immune responses could be
18 beneficial in vaccines. The current approved SARS-CoV-2 vaccines target generation of
19 neutralizing antibodies and are robust strategies for establishing sterilizing immunity (Jeyanathan
20 et al., 2020); however, respiratory targeting could be considered for individuals who are unable
21 to develop effective antibody responses. These cohorts may include the immunocompromised or
22 the elderly, or this strategy could be used as a booster for those at risk of infection due to
23 frequent interactions with others through their living or work situations. Indeed, a recent pre-

1 clinical study demonstrated that intranasal administration of a recombinant SARS-CoV-2
2 vaccine promoted lung TRM generation and protection from viral challenge in mice (Hassan et
3 al., 2020).

4 In summary, our study provides a dynamic view of ongoing respiratory and systemic
5 immunity in severe COVID-19, revealing key roles for airway immune cells in promoting
6 protection and driving lung inflammation. These findings have important implications for how
7 we monitor, treat and protect from this pandemic and future infectious challenges to the
8 respiratory tract.

9 **Limitations of Study**

10 Limitations of this study include a small cohort size and short sampling window (up to 10
11 days after intubation) during a course of prolonged acute illness. Due to the small sample size
12 and the older age of patient who died, we were not able to separate the role of age and immune
13 cell frequencies with outcome. However, the strong inverse correlation that we observed between
14 age and lower T cell frequencies suggests that there are age-related changes in airway immunity
15 that may explain the higher mortality observed in older adults with severe COVID-19. Moreover,
16 we only studied respiratory and blood responses in severe COVID-19, and not in more mild
17 manifestations of the disease, and it will be interesting in future studies to incorporate upper
18 respiratory sampling to assess immunity during a resolved infection.

19

1 **Acknowledgements**

2 We wish to express our gratitude to the Medical ICU nurse champions, Cora Garcellano, Tenzin
3 Drukduk, Harriet Avila Raymundo, Lori Wagner, and Ricky Lee, who led the efforts to obtain
4 patient samples for the severe COVID-19 patients, to Evelyn Hernandez and Lorena Gomez for
5 their roles as clinical coordinators, and to the nurses and clinical staff in the Pediatric Intensive
6 Care Unit of MSCHONY. We acknowledge the dedication, commitment, and sacrifice of the
7 other nurses, providers, and personnel who helped care for these patients during the COVID-19
8 crisis. We acknowledge the suffering and loss of our COVID-19 patients and of their families
9 and our community. We gratefully acknowledge the generosity of the donor families and the
10 exceptional efforts of LiveOnNY transplant coordinators and staff for the organ donor lungs.

11 This work was supported by NIH grants AI128949 and AI06697 awarded to D.L.F., a
12 Chan Zuckerberg Initiative COVID-19 grant to D.L.F. and P.A.Sims, and an R01AI093870
13 awarded to A.J.Y. P.D. was supported by a CRI-Irvington Postdoctoral Fellowship and P.A.S. by
14 a Canadian Institutes of Health Research Fellowship. T.J.C. is supported by NIH K23 A1141686
15 and S.P.W. is supported by NIH K08 DK122130. Research reported in this publication was
16 performed in the Human Immune Monitoring Core, the Columbia Single Cell Analysis Core, and
17 the Sulzberger Columbia Genome Center, which are supported by an NCI cancer center support
18 grant P30CA013696. The content is solely the responsibility of the authors and does not
19 necessarily represent the official views of the National Institutes of Health. We thank Eldad Hod
20 for use of his laboratory for sample processing, and Carly Ziegler and Dr. Alex Shalek of MIT
21 for sharing their merged human SARS-CoV-2 genome and transcriptome annotation.

22 **Author Contributions**

1 P.A.Sz., S.B.W., J.G., P.D. processed samples, designed and optimized high-dimensional flow
2 cytometry panels, analyzed data, made figures, and wrote the manuscript. P.A.Sz. and S.B.W.
3 processed samples for scRNA-seq profiling and encapsulation using 10X Chromium; I.K.
4 prepared and sequenced the 10X libraries. P.D. designed the Python pipeline for flow cytometry
5 data. M.B. monitored and consented ICU patients, oversaw clinical data analysis and collected
6 samples. T.C. obtained and maintained IRB protocols, consented patients, and processed
7 samples. M.M.L.P., R.M., E.I., M.C. obtained and processed patient samples. S.E.M., C.P., and
8 A.J.Y. statistically analyzed longitudinal data and performed k-means clustering analysis; J.D.-P.
9 captured and analyzed patient data; J.Z., M.S. S.M. performed cytokine analysis of airway
10 supernatants and blood plasma; S.P.W. planned, designed, and analyzed lung autopsy imaging
11 experiments; A.S. provided lung autopsy samples and associated data; A.K. performed
12 immunohistochemistry of lung autopsies. P.A.Sims planned scRNA-seq experiments, analyzed
13 data, and wrote and edited manuscript. D.L.F. oversaw compliance, planned experiments,
14 coordinated sample acquisition and data acquisition/analysis, analyzed data, and wrote and
15 edited the paper.

16 **Declaration of Interests**

17 J.Z., M.S. and S.M. have competing interests with IsoPlexis. The remaining authors declare no
18 competing interests.

1 **FIGURE LEGENDS**

2 **Figure 1. Immune cell composition in airway and blood compartments of COVID-19**

3 **patients compared to healthy controls.** (A) Schematic diagram showing assays performed on

4 COVID-19 patient airway and blood samples for this study. (B) Principal component analysis

5 (PCA) of all COVID-19 samples based on mean marker expression colored by site (left),

6 condition (middle) and by subjects (right). (C) UMAP embedding of flow cytometry results from

7 all airway and blood samples combined colored by major cell lineage (top panel), and separated

8 by tissue site in COVID-19 and healthy donor samples (bottom four panels) (COVID-19 airway:

9 $n = 69$, COVID-19 blood: $n = 83$, healthy airway: $n = 5$, healthy blood: $n = 5$). (D) Box plots

10 showing the frequency of major immune cell lineages of total $CD45^+CD66B^-$ cells in COVID-19

11 and healthy airway (left) and blood (right) samples. Each dot in the boxplot represents an

12 individual patient sample. Statistical significance was calculated using one-way ANOVA

13 followed by Tukey's HSD post-test indicated by ***, $p \leq 0.001$; **, $p \leq 0.01$; *, $p \leq 0.05$. (E)

14 Box plots showing the frequency of each major cell lineage of total $CD45^+CD66B^-$ cells in

15 airway (top) and blood (bottom) samples collected longitudinally for COVID-19 and healthy

16 subjects. Color of boxes corresponds to lineage and each dot is an individual patient sample.

17

18 **Figure 2. Longitudinal assessments of immune cell composition and association with age**

19 **and outcome.** (A) Correlation of immune cell frequencies in the airways (left) and blood (right)

20 with age. Each dot represents the mean immune cell frequency for each patient from all time

21 points, and color denotes patient outcome: survived (blue), deceased (red). Statistical

22 significance was calculated by Spearman correlation (indicated by rho) with p-value shown in

1 each graph. (B) Daily frequencies of immune cells in the airway (left) and blood (right) for each
2 patient over time stratified by deceased and survived. Solid red and blue lines show mean cell
3 lineage frequency for deceased and survived patients, respectively. Area-under-the-curve (AUC)
4 normalized for number of sampling days was calculated for each patient, and mean AUC is
5 shown in each graph. Statistical significance was calculated by one-tailed Mann-Whitney U tests
6 (see methods) for the AUC with Benjamini-Hochberg correction for multiple comparisons and is
7 denoted by *, $p \leq 0.05$. (C) K-means trajectory clustering analysis of clinical and immune cell
8 frequencies with outcome. *Left*: Representative trajectories of P/F ratio, SOFA score, airway
9 myeloid cells, and airway CD4⁺ T cells for all patients used for k-means clustering and
10 classification. The true outcome of each patient is denoted by red (deceased) or blue (survived)
11 lines and inferred clustering by k-means is denoted by solid (deceased) or dashed (survived)
12 lines. Correct clustering denoted by red solid lines and blue dashed lines. *Right*: Patient outcome
13 classification performance of longitudinal K-means clustering for different combinations of
14 immune cell trajectories and clinical parameters (SOFA score and P/F ratio). The percentage of
15 patient outcomes successfully classified as deceased or survived is shown for each parameter
16 measured in airway (gray) or blood (black). Dotted red line indicates classification performance
17 by the P/F ratio and SOFA score.

18

19 **Figure 3. Airway T cells in COVID-19 are dominated by TRM and activated phenotypes.**

20 (A) Heatmap displaying expression of markers within Phenograph-generated, hierarchical T cell
21 clusters. 24 Phenograph clusters were collapsed into 13 definable T cell subsets indicated along
22 the top. Heatmap data are colored by row normalized value for each marker. (B) UMAP
23 embeddings of T cell subsets (as defined in A) in the blood and airways of COVID-19 patients

1 and healthy controls (first and third row). Pie charts indicating relative proportions of defined T
2 cell subsets in airway and blood of COVID-19 patients and healthy controls (second and fourth
3 rows). (C) T cell subset frequencies in airway and blood samples from COVID-19 patients
4 (n=13) and healthy controls (n=5). Boxplots show the frequency of the indicated T cell subset for
5 each patient (average of all time points per patient) or healthy controls. Statistical significance
6 was calculated using a one-way ANOVA with Tukey's test for multiple comparisons and
7 indicated by ***, $p \leq 0.001$; **, $p \leq 0.01$; *, $p \leq 0.05$. (D) Expression of T cell activation markers
8 HLA-DR and PD-1 on T cells (total CD3⁺ cells) from blood and airways of COVID-19 patients
9 and healthy controls. *Left*: contour plots showing mean expression on HLA-DR and PD-1 on T
10 cells from each cohort, with airway contours colored in blue and blood colored in red. *Right*:
11 frequency of T cells expressing HLA-DR and PD-1 in the airway and blood for each COVID-19
12 patient (n=13; averaged over all time points) or healthy controls (n=5). Statistical significance
13 was calculated using a one-way ANOVA with Tukey's test for multiple comparisons and
14 indicated by ***, $p \leq 0.001$.

15

16 **Figure 4. Dysregulated myeloid cell subsets in the blood and airways of COVID-19 patients**

17 (A) Heatmap displaying expression of markers within Phenograph-generated, hierarchical
18 myeloid cell clusters. 21 Phenograph clusters were collapsed into 9 definable subsets indicated
19 above the heatmap. Heatmap data are colored by value normalized to that of T cell expression as
20 an internal negative control for each sample. (B) UMAP embedding of 9 myeloid cell subsets in
21 the airway (left) and blood (right) of COVID-19 (upper) and healthy controls (lower) with colors
22 denoting the specific subset as defined in (A) (first and third rows). Pie charts indicating relative
23 proportions of defined myeloid cell subsets in airway and blood of COVID-19 patients and

1 healthy controls (second and fourth rows). (C) Boxplots showing compiled frequency of each
2 myeloid subset displayed as an average of all time points collected for COVID-19 samples (CA
3 – COVID-19 Airway, CB – COVID-19 Blood, HA – Healthy Airway, HB – Healthy Blood). (D-
4 F) Expression of myeloid markers in airway and blood shown as contour plots of expression of
5 indicated markers by myeloid cells in airway (blue contours) and blood (red contours) samples
6 by condition (healthy or COVID-19). Boxplots (to the right or below the contour plots) indicate
7 percentage of cells within each condition and site that were positive for specific markers.
8 Statistical significance was calculated using a one-way ANOVA followed by a Tukey HSD and
9 indicated by ***, $p \leq 0.001$; **, $p \leq 0.01$; *, $p \leq 0.05$.

10

11 **Figure 5. Inflammatory gene signatures of T cells and myeloid cells are enriched in the**
12 **airways of COVID-19 patients.** T cells and monocytes/macrophages from the blood and
13 airways of COVID-19 patients were analyzed by scRNA-seq (see methods). (A) Separate UMAP
14 embeddings showing gene expression from total T cells obtained from airway and blood of
15 paired samples from four patients. UMAP embeddings show sample site origin, subject and
16 indicated gene expression (based on $\log_2(\text{CPM}+1)$). (B) Heatmap showing major differentially
17 expressed genes in airway compared to blood T cells from each individual patient and timepoint.
18 Data are colored by row z-scored $\log_2(\text{CPM}+1)$ for each sample. (C) UMAP embeddings of total
19 monocyte/macrophage cells obtained from airway and blood from four COVID-19 patients.
20 UMAP embeddings show sample site origin, patient, and selected gene expression displayed as
21 $\log_2(\text{CPM}+1) / \text{maximum}$. (D) Heatmap of subset-defining genes, homing receptors and key
22 inflammatory molecules for monocyte/macrophages in airway and blood from each patient
23 sample. The heatmap shows genes that are not differentially expressed between airway and blood

1 (*CD14-FCGR3A*) and genes are consistently differentially expressed (*ITGAV-TREM2*).

2

3 **Figure 6. COVID-19 airways contain highly elevated levels of myeloid and T cell-derived**

4 **cytokines** (A) Pairwise comparison of cytokine levels averaged across both timepoints in airway

5 wash and blood plasma samples collected from 15 patients. Significance indicated as: p-value \leq

6 $0.05 = *$, p-value $\leq 0.01 = **$ and p-value $\leq 0.001 = ***$. (B) Heatmap showing $\log_{10}(\text{mean } X+1)$

7 pg/mL cytokine levels averaged across both time points in airway (left) and blood plasma (right)

8 samples for each patient. (C) Transcript levels for cytokine expression by major cell lineages

9 identified in by scRNA-seq for each patient samples indicated by color. Heatmap shows

10 $\log_2(\text{mean CPM}+1)$ gene expression.

11

12 **Figure 7. COVID-19 lung autopsies exhibit specific and extensive accumulation of**

13 **monocyte/macrophages relative to control lungs.** (A) Lung sections obtained from non-

14 diseased organ donors and autopsy specimens from COVID-19 patients with diffuse alveolar

15 damage were stained with indicated antibodies and analyzed using Vectra. Representative

16 images show staining for CD19 (B cell), CD4 or CD8 (T cells), CD163

17 (monocytes/macrophages), MMP9 (neutrophil) and granzyme B (cytotoxicity) in the lungs of

18 uninfected controls (left) and COVID-19 patients (right). (B) Quantitation of immune cell

19 subsets in (A) for uninfected organ donor lungs (n=3) and COVID-19 lungs (n=5) as a frequency

20 of total lung cells (top) or density (bottom; cells per mm^2 cellular area) using InForm software.

21 Statistical significance calculated by paired T-test and indicated by *, $p \leq 0.05$. (C) UMAP

22 embedding showing expression of genes associated with proliferation by scRNA-seq in

23 monocyte/macrophages derived from airway and blood as in Figure 5.

1 **STAR Methods**2 **KEY RESOURCES TABLE**

REAGENT or RESOURCE	SOURCE	IDENTIFIER
Antibodies		
Spectral Flow Cytometry		
Anti-Human HLA-DR BU395	BD	G46-6; Cat No.:564040
Anti-Human CD16 BU496	BD	3G8; Cat No.:612944
Anti-Human CD163 BU563	BD OptiBuild	GHI/61; Cat No.:741402
Anti-Human CD33 BU615	BD OptiBuild	WM53; Cat No.:751275
Anti-Human PD-1 BU661	BD OptiBuild	EH12.1; Cat No.:750260
Anti-Human CD56 BU737	BD	NCAM16.2; Cat No.:612766
Anti-Human CD64 BU805	BD OptiBuild	10.1; Cat No.:742023
Anti-Human CCR7 BV421	BioLegend	G043H7; Cat No.: 353208
Anti-Human CD86 SB436	eBioscience	IT2.2; Cat #62-0869-42
Anti-Human CD28 eFluor 450	eBioscience	CD28.2; Cat #48-0289-42
Anti-Human CD8 BV480	BD	RPA-T8; Cat No.:566121
Anti-Human CD20 Pacific Orange	Invitrogen	HI47; Cat #MHCD2030
Anti-Human CD3 BV510	BioLegend	UCHT1; Cat #300448
Anti-Human CD45RA BV570	BioLegend	HI100; Cat #304132
Anti-Human CD25 BV605	BioLegend	BC96; Cat #302632
Anti-Human CD27 BV650	BioLegend	O323; Cat #302828
Anti-Human CD69 BV711	BioLegend	FN50; Cat #310944
Anti-Human CXCR5 BV750	BD OptiBuild	RF8B2; Cat No.:747111
Anti-Human CD335 BV785	BioLegend	9E2; Cat #331946
Anti-Human CD103 BB515	BD	Ber-ACT8; Cat No.:564578
Anti-Human CD66b FITC	BioLegend	G10F5; Cat #305104
Anti-Human CD14 Spark Blue 550	BioLegend	63D3; Cat #367148
Anti-Human CD45 PerCP	BioLegend	HI30; Cat #304026
Anti-Human CD57 PerCP-Cy5.5	BioLegend	HNK-1; Cat #359622
Anti-Human TCR gamma/delta PerCP-eFluor 710	eBioscience	B1.1; Cat #46-9959-42
Anti-Human CD138 PE	BioLegend	MI15; Cat #356504
Anti-Human CD4 YG584	Cytek	SK3; Cat #R7-20041
Anti-Human CD123 PE-CF594	BioLegend	6H6; Cat #306034
Anti-Human CD95 PE-Cy5	BioLegend	DX2; Cat #305610
Anti-Human CD11c PE-Cy7	BioLegend	3.9; Cat #301608
Anti-Human CD19 Spark NIR 685	BioLegend	HIB19; Cat #302270
Anti-Human CD127 APC-R700	BD	HIL-7R-M21; Cat No.:565185
Anti-Human KLRG1 APC/Fire 750	BioLegend	SA231A2; Cat #367718
Anti-Human FoxP3 Alexa Fluor 647	BioLegend	259D; Cat #320214
Multispectral staining of lung tissue		
Anti-human CD19	Leica	BT51E; Cat #CD19-163-L-CE
Anti-human CD8	Leica	4B11; Cat #CD8-4B11-L-CE
Anti-human CD163	Leica	10D6; Cat #CD163-L-CE
Anti-human CD4	Abcam	EPR6855; Cat #ab133616
Anti-human GzmB	Leica	11F1; Cat #GRAN-B-L-CE

Anti-human MMP9	Santa Cruz Biotechnology	2C3; Cat #sc-21733
Biotinylated Antibodies		
Anti-human CD66b Biotin	BioLegend	G10F5; Cat #305120
Anti-human CD235b Biotin	BioLegend	HIR2; Cat #306618
Chemicals, Peptides, and Recombinant Proteins		
LIVE/DEAD Fixable Blue Dead Cell Stain	Thermo Fisher Scientific	Cat #L23105
DAPI	BioLegend	Cat #422801
True-Stain Monocyte Blocker	BioLegend	Cat #426102
TrueStain FcX	BioLegend	Cat #422302
RPMI 1640	Corning	Cat #10-040-CM
Ficoll-Paque PLUS	GE	Cat #17-1440-03
RosetteSep Granulocyte Depletion Cocktail	STEMCELL Technologies	Cat #15624
Benzonase	Millipore Sigma	Cat #E1014-5KU
DPBS	Corning	Cat #20-030-CV
EDTA	Corning	Cat #46-034-CI
Foxp3 / Transcription Factor Staining Buffer Set	eBioscience	Cat #00-5523-00
10% Zinc Formalin	Anatech	Cat # 170
Vectashield Hard Set mounting media	Vector Labs	Cat #H1600
Opal 7-Color IHC Kits	Akoya Biosciences	Cat #NEL811001KT
Critical Commercial Assays		
Chromium Next GEM Single Cell 3' Reagent kit v3.1	10x Genomics	https://support.10xgenomics.com/single-cell-gene-expression/library-prep
Deposited Data		
scRNA-seq Data	This article	https://www.covid19cellatlas.org/index.patient.html
Software and Algorithms		
Python version 3.7	Python (2020)	https://www.python.org/downloads/release/python-370/
Anaconda version 4	Anaconda (2020)	https://www.anaconda.com/products/individual
Rstudio version 1.2.1335	RStudio, Inc. (2019)	https://www.rstudio.com
R version 3.5	R Foundation for Statistical Computing (2017)	https://www.R-project.org
inform Version 2.3	Perkin Elmer, Akoya Biosciences	https://www.akoyabio.com/phe-noptics/software/inform-tissue-finder/
FlowJo V 10.7 software	Tree Star	https://www.flowjo.com/
Other		

Dead Cell Removal Microbeads	Miltenyi Biotec	Cat #130-090-101
BioMag Plus Streptavidin	Bangs Labs	Cat #BP628

1

2 **RESOURCE AVAILABILITY**

3

4 **Lead contact**

5 Further information and requests for reagents should be directed to and will be fulfilled by lead
6 author Donna L. Farber (df2396@cumc.columbia.edu)

7

8 **Materials availability**

9 This study did not generate new unique reagents.

10

11 **Data and code availability**

12 The scRNA-seq data for each sample including count matrices, normalized counts, metadata, cell
13 annotations, and UMAP embeddings are available on the COVID-19 Cell Atlas along with
14 interactive visualizations (<https://www.covid19cellatlas.org/index.patient.html>). Code for
15 clustering of scRNA-seq data analysis is available at
16 www.github.com/simslab/cluster_diffex2018. Additional Supplemental Items are available from
17 Mendeley Data at 10.17632/fm7v43jrbk.3

18

19 **EXPERIMENTAL MODEL AND SUBJECT DETAILS**

20 **Human samples**

21 We recruited patients from and CUIMC/NYP and Morgan Stanley Children's Hospital of NY
22 with severe COVID-19 and ARDS (n=15) who tested positive for SARS-CoV-2 by polymerase

1 chain reaction (PCR) from nasopharyngeal swabs (Table S1, S2). Blood and airway sampling
2 began within 24-36 hours for all patients. ARDS was defined by clinical consensus criteria
3 including infiltrates on chest radiograph and a PaO₂/FiO₂ (P/F) ratio of less than 300, or
4 pediatric criteria equivalent (Khemani et al., 2015; Ranieri et al., 2012). Exclusion criteria
5 included patients with cancer, transplant recipients, immunodeficiencies, and existing bacterial
6 infection. Sequential Organ Failure Assessment (SOFA) scores were calculated on all
7 hospitalized patients using previously validated adult and pediatric score tools to provide
8 additional clinical insight into patient disease severity (Matics and Sanchez-Pinto, 2017; Singer
9 et al., 2016; Vasilevskis et al., 2016). All patients and samples in this study were enrolled on
10 protocols approved by the Institutional Review Board at CUIMC. Due to the limitations placed
11 on direct contact with infected patients and a need to conserve personal protective equipment,
12 verbal informed consent was obtained from surrogates of critically ill COVID-19-ARDS
13 patients.

14 Paired airway and blood samples were obtained from COVID-19 patients enrolled as
15 above daily or every second day up to 7-10 days; the number of samples obtained varied due to
16 patient death or extubation. Airway samples were collected from saline washes of the
17 endotracheal tube during routine clinical care and blood samples were obtained by venous
18 puncture. Healthy blood was obtained from 5 adult volunteers 31-57 years.

19 Control, uninfected lung tissues were obtained from deceased organ donors (who died > 2
20 years before the pandemic) as part of organ acquisition for clinical transplantation through an
21 approved protocol and material transfer agreement with LiveOnNY as described previously
22 (Carpenter et al., 2018; Dogra et al., 2020). Donors were free of cancer, chronic diseases,
23 seronegative for hepatitis B, C, and HIV, and negative for SARS-CoV-2 by PCR (Table S7). Use

1 of organ donor tissues does not qualify as “human subjects” research, as confirmed by the
2 Columbia University IRB as tissue samples were obtained from brain-dead (deceased)
3 individuals.

4 5 **METHOD DETAILS**

6 **Processing of blood samples and isolation of PBMCs from COVID-19 patients**

7 Whole blood collected in heparinized vacutainers was centrifuged at 400 x g for 10 min at room
8 temperature (RT) to isolate plasma, which was then stored at -80°C for subsequent analysis.
9 PBMCs were isolated using Ficoll-Paque PLUS (GE) density gradient centrifugation in a
10 Biosafety Level 2+ facility. To remove neutrophils, blood was incubated with RosetteSep
11 Granulocyte Depletion Cocktail (Stemcell Technologies), diluted 1:3 in room temperature DPBS
12 (Corning), layered over Ficoll-Paque PLUS in 50mL conical tubes, and centrifuged for 20 min at
13 1,200 x g. The PBMC layer was isolated according to the manufacturer’s instructions. Cells were
14 washed twice with DPBS before counting with the automated NucleoCounter NC-3000 cell
15 counter (ChemoMetec).

16 17 **Processing of airway samples and isolation of airway MNCs from COVID-19 patients**

18 Both the cellular content and supernatants were collected from airway samples. To collect airway
19 supernatants, DPBS was added 1:1 directly to airway samples and centrifuged at 400 x g for 10
20 min at RT. The resulting supernatants were stored at -80°C for subsequent analysis. To isolate
21 airway MNCs, samples were treated with Benzonase (Millipore Sigma), purified through 100
22 μm filters, and centrifuged on a density gradient using Ficoll-Paque PLUS. The MNC layer was

1 isolated according to the manufacturer's instructions. Cells were washed twice with DPBS
2 before counting with the automated NucleoCounter NC-3000 cell counter.

3

4 **Cell preparation for scRNA-seq, library generation and sequencing**

5 Airway and blood MNC populations were isolated as above, and the remaining neutrophils and
6 red blood cells were removed by incubating samples with biotinylated anti-CD66b and anti-
7 CD235ab antibodies, and depleting antibody-bound cells with streptavidin-coated magnetic
8 beads (Bangs Labs). Dead cells were subsequently removed using the Dead Cell Removal kit
9 (Miltenyi Biotec). The Next GEM Chromium Controller (10x Genomics) and Chromium Next
10 GEM Single Cell 3' Reagent kit v3.1 (10x Genomics) was used for co-encapsulation and
11 scRNA-seq library construction as per manufacturer's suggested protocols. Libraries were
12 sequenced on an Illumina NovaSeq 6000, targeting ~300M raw reads per sample (~60,000 raw
13 reads per cell). Sample details and number of cells sequenced in each are shown in Table S3.

14

15 **Isolation of airway washes from non-diseased lungs**

16 Uninfected lungs were obtained from deceased organ donors as described above. Airway washes
17 were obtained by flushing out the major airway with 60 mL saline as described (Snyder et al.,
18 2019). Cells were pelleted by centrifugation, resuspended in DPBS and stained with antibodies
19 for flow cytometry.

20

21 **High-dimensional flow cytometry**

22 For high parameter analysis using the Cytex Aurora panel, 5×10^6 cells from each site were
23 stained in 5 mL U-bottom tubes in the dark using antibody panels as described in the Key

1 Resources Table. Briefly, cells were first washed with DPBS, re-suspended with LIVE/DEAD
2 Fixable Blue Dead Cell stain (Thermo Fisher Scientific) and incubated at RT in the dark for 30
3 min. Following incubation, cells were washed with cold FACS-buffer (DPBS + 2% FBS + 0.1
4 mM EDTA) and re-suspended with human TrueStain FcX and True-Stain Monocyte Blocker
5 (BioLegend) and incubated in the dark for 10 minutes. Following incubation, were incubated
6 with a cell-surface marker staining cocktail as described in Key Resources Table at 4 °C for 30
7 min. Stained cells were washed twice with cold FACS-buffer to remove unbound antibodies. For
8 intracellular staining, cells were fixed, permeabilized and stained with intracellular antibodies
9 (Key Resources Table) using a Foxp3 Transcription Factor Staining Buffer Set (eBioscience) as
10 per manufacturer's suggested protocols. Cells were incubated in the dark for 30 minutes with
11 intracellular antibodies and washed twice. Data was collected on 5-laser Cytex Aurora flow
12 cytometer (Cytex Bio).

13

14 **Highly-multiplexed CodePlex chip secretome proteomics**

15 Cryopreserved tracheal washes and plasma were thawed at room temperature for 30-60 minutes
16 and mixed well by pipetting up and down prior to loading. An aliquot of 5.5 μ L of each sample
17 was pipetted into each macrochambers of a CodePlex chip pre-patterned with a complete copy of
18 a 23-plex antibody array. 2% BSA/PBS was used as background control. The chip was then
19 loaded into an IsoLight automation system and various proteins were measured by fluorescence
20 ELISA and analyzed by the IsoSpeak software using the IsoPlexis Human Adaptive Immune
21 Panel: GM-CSF, Granzyme B, IFN- γ , IL-10, IL-13, IL-15, IL-17A, IL-2, IL-4, IL-5, IL-6, IL-7,
22 IL-8, IL-9, IP-10, MCP-1, MIP-1 α , MIP-1 β , Perforin, sCD137, TGF- β 1, TNF- α , TNF- β .

23

1 **Multispectral staining and imaging of lung tissue**

2 Representative samples of lung tissue 0.5–1.0 cm in thickness were obtained from organ donors
3 and autopsy cases of individuals diagnosed with COVID-19 and found on post-mortem exam to
4 have pathological findings consistent with diffuse alveolar damage (Table S7). Uninfected lung
5 sections were obtained from deceased organ donors who were brain dead due to trauma >2 years
6 prior to the pandemic. None of the donors used for the control staining in Figure 7 showed
7 pathological evidence of lung damage or diffuse alveolar damage.

8 Samples were fixed in 10% formalin (Anatech Ltd.) for 48 hours prior to dehydration and
9 embedding in paraffin. These lung samples were sectioned at 5-mm thickness and stained using
10 7-color multispectral Opal reagents (Akoya Biosciences) as previously described (Gartrell et al.,
11 2018; Weisberg et al., 2019). The multiplex panel included DAPI for nuclear counterstaining,
12 CD4 (1:150 dilution), CD8 (1:600 dilution), CD163 (1:200 dilution), granzyme B (GzmB)
13 (1:200 dilution), CD19 (1:50 dilution), MMP9 (1:900 dilution). Single controls and an unstained
14 slide were stained with each group of slides. After staining, the sections were mounted in
15 Vectashield Hard Set mounting media (Vector Labs, Cat#H1600) and stored at 4⁰C for up to 48
16 hours prior to image acquisition. Multispectral imaging and acquisition at 20x magnification
17 (numerical aperture 0.75) was performed using the integrated Vectra 3 automated quantitative
18 pathology imaging system (PerkinElmer) as previously described (Weisberg et al., 2019). Images
19 were analyzed using inForm software (PerkinElmer/Akoya Biosciences). Representative areas
20 (10-30) from each donor were chosen for quantitative analysis.

21

22 ***Flow cytometry analysis***

23 Flow cytometry data was pre-gated to exclude any doublets, dead cells and CD66b⁺ granulocytes

1 using FlowJo v 10.7 (Tree Star) (Figure S1). Cleaned data was exported as .fcs files with
2 compensated parameters and analyzed further and visualized using a Python (v3.7) (Python
3 Software Foundation. Python Language Reference, version 2.7.) computational pipeline. In brief,
4 first the data was filtered to remove any noise using quantile gates; events that fell below 0.01%
5 of marker expression intensity were removed from the sample. Following initial filtering, data
6 from COVID-19 and healthy samples was merged after subsetting 60,000 events from each
7 COVID-19 airway and blood sample, 120,000 events from each healthy blood sample, and all
8 events from healthy airway samples. Any sample with fewer than 1000 events was removed
9 from further analysis. The merged dataset was transformed using arcsinh function from Python
10 *numpy* library(van der Walt et al., 2011) after manually adjusting the cofactor for each marker.
11 Following normalization, the dataset was normalized on a 0-1 feature scale for each marker
12 using *MinMaxScaler* function from Python *scikit-learn* library (Pedregosa et al., 2011). The
13 cleaned, transformed and scaled dataset was used to run the first round of *Uniform Manifold*
14 *Approximation and Projection* (UMAP) (McInnes et al., 2018) dimensionality reduction to
15 remove any residual granulocyte contamination identified as clusters of CD45^{lo}CD66b⁺ cells.
16 The resulting dataset was used for downstream analysis.

17 We ran PCA analysis at sample level using mean expression of markers in each sample,
18 PCA loadings provided in Table S3. Next, we ran UMAP dimensionality reduction (k = 60) on
19 this dataset using 10 lineage-defining markers (CD14, CD16, CD19, CD3, CD33, CD4, CD8,
20 CD64, CD56, CD335). The data were projected in 2-dimensions using UMAP embeddings and
21 clusters of major immune cell types (CD4 and CD8 T cells, B cells, NK/ILC and Myeloid cells)
22 were identified based on expression of lineage defining markers (Figure S2A). Frequency of the
23 major lineages was calculated for each donor sample.

1 For immune cell lineage and age analyses (Figure 2A, Figure S2A), the average
2 frequency values across all timepoints for each patient was calculated and plotted relative to age,
3 showing spearman's rho values with corresponding p value. For longitudinal analyses of immune
4 cell frequencies between deceased and surviving patients (Figure 2B), area-under-the-curve
5 (AUC) was calculated for each patient and divided by the number of sampling days (omitting
6 COV007 who was sampled for one day only). Statistical significance between deceased and
7 survived groups was calculated based on AUC using a one-tailed Mann-Whitney U test, testing
8 the specific hypothesis that increased protective responses (T cells) are associated with positive
9 outcomes (D<S) and increased pro-inflammatory responses (myeloid cells) would be associated
10 with negative outcomes (D>S). We applied a Benjamini-Hochberg correction for multiple
11 comparisons.

12 For lineage specific analysis (T cells, myeloid cells), we ran UMAP dimensionality
13 reduction and subsequent *Phenograph* clustering (Levine et al., 2015) on each lineage specific
14 dataset using cell subset defining markers selected based on literature review. Markers used for T
15 cell UMAP are shown in Figure S4A. Myeloid cell markers are shown in Figure S5A. Major cell
16 subset clusters were identified and functionally similar subsets were coalesced and manually
17 annotated. Heatmaps were generated for average marker expression in each of the annotated
18 clusters. Data are presented as row normalized expression of marker across all clusters. All
19 graphs were generated using the Python *matplotlib* and *seaborn* libraries (Hunter, 2007).

20

21 ***Classifying patient outcomes using longitudinal K-means clustering***

22 Patients were partitioned into two groups using a longitudinal K-means algorithm applied to the
23 trajectories of the frequencies of myeloid, B cell, CD4 and CD8 T cell and ILCs in blood or

1 airways in addition to the trajectories of SOFA score and P/F ratio. The proximity of two
2 patients' trajectories was defined using the sum of the squared Euclidean distances between their
3 subset frequencies at each location at each timepoint, after normalizing each subset frequency
4 across all patients and timepoints. The clustering outcome was robust to this definition of
5 distance, giving identical results when performed using log- or logit-transformed frequencies.
6 Classification performance was defined as the percentage of patients that were assigned to the
7 correct outcome cluster (deceased or survived). We compared the abilities of different immune
8 cell subsets to distinguish patient outcome by repeating the clustering analysis on different
9 combinations of trajectories. Greater classification performance indicated increased power to
10 identify patient outcomes. Clustering analyses were conducted in *R* version 3.5.3 using the *kml3d*
11 package, version 2.4.2, and the results were visualized using the *ggplot2* package.

13 ***Processing of scRNA-seq Data***

14 We used kallisto v0.46.2 in "BUS" mode to pseudo-align the raw reads for each sample to a
15 merged human GRCh38 (Ensembl 93)/SARS-CoV-2 transcriptome (Bray et al., 2016; Kim et al.,
16 2020; Melsted et al., 2019a; Melsted et al., 2019b). To correct for index swapping, which can
17 occur on the Illumina NovaSeq 6000, we applied the algorithm of Griffiths *et al* (Griffiths et al.,
18 2018) to the equivalence classes obtained from kallisto pseudo-alignment. We generated a raw
19 count matrix from the swap-corrected BUS file using bustools v0.40.0 (Melsted et al., 2019b),
20 filtered using the EmptyDrops algorithm (Lun et al., 2019), and removed all cells with
21 mitochondrial pseudo-alignment rates >20% or counts per gene greater than two standard
22 deviations above the mean for each sample.

23

1 *scRNA-Seq Cell Annotation*

2 We merged the scRNA-seq data from all of the airway samples and identified likely markers of
3 specific subpopulations using the previously described drop-out score method for finding genes
4 that are detected in fewer cells than expected given their expression level (Levitin et al., 2019;
5 Szabo et al., 2019). Next, we computed a cell-by-cell Spearman's rank correlation matrix using
6 these putative marker genes. Using this matrix, we constructed a k-nearest neighbor's graph
7 (k=20) as input for Louvain community detection as implemented in Phenograph (Levine et al.,
8 2015). To associate the resulting clusters with major cell populations in the airway, we examined
9 the statistical enrichment of the following marker genes in each cluster using the binomial test as
10 described in Shekhar *et al* (Shekhar et al., 2016): T cells (*CD3D*, *TRAC*, *TRBC1*, *TRBC2*, *TRDC*,
11 *TRGC1*, *TRGC2*), NK cells (*NCAM1*), myeloid cells (*CD14*, *FCGR3A*, *CD163*),
12 epithelial/club/goblet cells (*EPCAM*, *SCGB1A1*, *MUC5B*, *KRT78*), ionocytes (*CFTR*),
13 neutrophils (*CD16B*), plasma cells (*CD19*, *JCHAIN*), B cells (*CD19*, *MS4A1*), platelets
14 (*ITGA2B*, *PF4*), mast cells (*KIT*), dendritic cells (*FCER1A*, *CD1C*) and red blood cells (*HBA1*,
15 *HBA2*, *HBB*). We identified clusters as likely multiplets based on co-expression of multiple
16 marker sets (e.g. clusters enriched in both *CD14* and *CD3D* were marked as likely T cell /
17 myeloid cell multiplets). All of the cells in these clusters were marked as multiplets. UMAP
18 embeddings for all cells from each patient across all time points for airways and blood are shown
19 in Figure S5.

20 In the main text, we present focused analyses on myeloid cells, T cells, and
21 epithelial/club/goblet cells from the airway. To further refine our annotation, we re-clustered the
22 cells annotated as each of these three cell types separately using the methods described above.
23 We then re-analyzed the enrichment of cell type-specific markers in the resulting new clusters.

1 As expected, this focused re-analysis of each of these three major populations identified
2 additional putative multiplet clusters and cells that we likely mis-clustered in the initial merged
3 analysis. We conducted two rounds of re-clustering for each of these three major cell types to
4 produce a refined annotation. The top of Figure S6A shows a gene expression heatmap for key
5 marker genes in the merged airway data set colored by patient and cell type annotation. We
6 repeated the above procedure for the merged blood scRNA-seq profiles including a focused re-
7 clustering analysis of the cells that we originally annotated as myeloid and T cells for refinement.
8 The bottom of Figure S6A shows a gene expression heatmap for key marker genes in the merged
9 blood data set colored by patient and cell type annotation.

10

11 *scRNA-Seq Visualization and Differential Expression Analysis*

12 We generated merged UMAP embeddings for the blood and airway T cells (Figure 5A) and the
13 blood and airway myeloid cells (Figure 5C). In each case, we first identified genes that were
14 likely to contaminate either the myeloid or T cell profiles in either the blood or airway to avoid
15 including them in any of our downstream clustering, visualization, or differential expression
16 analysis. We conducted pairwise differential expression analysis between all of the cells
17 annotated as a cell type-of-interest (e.g. myeloid) and each group of cells with a different
18 annotation for the blood and airway from each patient separately. For each pairwise comparison,
19 we randomly subsampled the two groups of cells to the same cell number. Next, we randomly
20 subsampled the molecular counts for cells in the two groups such that they have the same
21 average number of counts per cell. We then generated a merged count matrix for the two groups
22 and applied the pooled normalization technique from the *scran* package of Lun *et al* using the
23 *computeSumFactors* function (Lun et al., 2016). Finally, we conducted a gene-by-gene, non-

1 parametric differential expression analysis using the Mann-Whitney U-test as implemented with
2 the function *mannwhitneyu* from the Python package *scipy*. We corrected the resulting p-values
3 for false discovery using the Benjamini-Hochberg Procedure with the function *multipletests* from
4 the Python package *statsmodels*. Using the results of pairwise differential expression analysis,
5 we generated a blacklist of genes for a given cell type by taking any gene with at least 10-fold
6 enrichment in a different cell type with $FDR < 0.001$ in at least two patients. We removed all
7 genes with any enrichment in the cell type-of-interest with $FDR < 0.001$ in any patient to avoid
8 eliminating patient-specific markers of the cell type-of-interest. The final blacklists for blood and
9 airway myeloid and T cells appear in Table S8.

10 For both myeloid and T cells, we took all of the cells in the data set that we had annotated
11 as each of these two cell types and used the drop-out score method described above to generate a
12 list of putative, highly variable marker genes for each patient. Next, we generated a merged
13 count matrix across all patients for a given cell type, which we normalized using the pooling
14 method of Lun *et al* as described above (Lun et al., 2016). We then generated a log-normalized
15 submatrix ($\log_2(\text{counts per million} + 1)$) containing the union of the marker gene sets identified
16 for each patient after removing genes on the airway and blood blacklists for the cell type-of-
17 interest. Using the *PCA* function in the Python package *scikit-learn*, we decomposed this
18 submatrix into its principal components. We used the 10 principal components with the largest
19 eigenvalues as input to the scRNA-seq batch correction algorithm Harmony (Korsunsky et al.,
20 2019). We made the function *HarmonyMatrix* aware of only the first 10 principal components
21 and the patient identifiers for each cell. Finally, we computed a two-dimensional embedding
22 using the Python implementation of the Uniform Manifold Approximation and Projection

1 (UMAP) algorithm (McInnes and Healy, 2018) and the Pearson correlation matrix of the
2 Harmony-corrected principal components. These embeddings appear in Figure 5.

3 For the differential expression analysis between blood and airway myeloid cells and
4 between blood and airway T cells, we used the Mann-Whitney U-test approach described above.
5 We removed genes on the blacklists described above for each cell type prior to subsampling,
6 normalization, and statistical testing. We also restricted this analysis to protein-coding genes and
7 removed all T cell receptor and immunoglobulin variable regions. We performed differential
8 expression separately on each pair of matched airway and blood samples (there are 12 patient
9 time points for which we have matched samples). Stringent criteria were used to select the
10 differentially expressed genes displayed in the heatmaps in Figure 5. For the myeloid cell
11 heatmap in Figure 5, a gene had to be differentially expressed with a fold-change of at least 4 in
12 either direction and $FDR < 0.001$ in at least 9 of the 12 matched sample pairs. For the T cell
13 heatmap in Figure 5, we applied the first two criteria, but required them in only 6 of the 12
14 matched sample pairs. Results for all of the pairwise differential expression analyses comparing
15 airway and blood T and myeloid cells can be found in Table S5 and Table S6, respectively.

16

17 *Analysis and visualization of cytokine data*

18 Non-log transformed cytokine expression data from both time points was averaged for airway
19 and plasma from each patient and used for paired-site analysis. Cytokine expression data from
20 early and late time points was \log_{10} normalized and visualized as box plots overlaid with
21 individual data points. The \log_{10} normalized data was averaged across both the time points was
22 also used to generate heatmaps for cytokine expression across individual patient samples. Graphs
23 were generated using the Python *matplotlib* and *seaborn* libraries (Hunter, 2007).

1

2 ***Lung tissue imaging analysis***

3 Tissue segmentation was performed using inForm software on 10-30 representative fields
4 (Version 2.3, PerkinElmer/Akoya Biosciences). Immune cell constituents within each tissue
5 segment were defined by the DAPI nuclear counterstain to define the nucleus of each cell, with
6 each associated membrane detected via presence of a specific stain (CD3, CD19, CD4, GzmB,
7 MMP9 and/or CD163). Cell segmentation was adjusted as previously described to accurately
8 locate all cells and minimize nuclear hypersegmentation and hyposegmentation (Weisberg et al.,
9 2019). Cells were then phenotyped by training the phenotyping algorithm of inForm software,
10 identifying: monocyte/macrophage (CD163+ magenta cells), T cells (CD4⁺ cyan cells and CD8⁺
11 orange cells), B cells (CD19⁺ yellow cells), neutrophils (MMP9⁺). The cell segmentation data
12 summary provided densities and numbers of each cell type in the lung tissue segments and the
13 full cell segmentation data file provided the X and Y coordinates of each phenotyped cell.

14

15 **QUANTIFICATION AND STATISTICAL ANALYSIS**

16 Differences in means between two sample groups were compared using two-tailed t-tests or two-
17 tailed Mann-Whitney U tests, except when testing specific directed hypotheses (one-tailed).
18 Pearson correlations were used to correlate age and immune cell frequencies. Multiple group
19 comparisons were done using ANOVA followed by Tukey's HSD post-test. For comparing
20 paired airway to blood values we used paired two tailed t-tests. All statistical tests were run using
21 custom scripts based on Python *sciPy* library (Jones et al., 2001) or R (version 3.5.3.). *P*-values
22 below 0.05 were considered as statistically significant. For all figures *** denotes p-value <
23 0.001, ** denotes p-value < 0.01, and * denotes p-value < 0.05.

1 **Supplementary Data**

2 **Table S5. Related to Figure 5.** Differential gene expression by T cells in airway versus blood
3 for each sample by scRNA-seq.

4 **Table S6. Related to Figure 5.** Differential gene expression by myeloid cells in airway versus
5 blood for each sample by scRNA-seq.

6 **Table S8. Related to Figures 5-7.** Blacklisted genes for a given cell type for the scRNA-seq
7 analysis.

8

1 **REFERENCES**

- 2 Aggarwal, N.R., King, L.S., and D'Alessio, F.R. (2014). Diverse macrophage populations
3 mediate acute lung inflammation and resolution. *Am J Physiol Lung Cell Mol Physiol* *306*,
4 L709-725.
- 5
6 Bharat, A., Bhorade, S.M., Morales-Nebreda, L., McQuattie-Pimentel, A.C., Soberanes, S.,
7 Ridge, K., DeCamp, M.M., Mestan, K.K., Perlman, H., Budinger, G.R., *et al.* (2016). Flow
8 Cytometry Reveals Similarities Between Lung Macrophages in Humans and Mice. *Am J Respir*
9 *Cell Mol Biol* *54*, 147-149.
- 10
11 Bray, N.L., Pimentel, H., Melsted, P., and Pachter, L. (2016). Near-optimal probabilistic RNA-
12 seq quantification. *Nature biotechnology* *34*, 525-527.
- 13
14 Carpenter, D.J., Granot, T., Matsuoka, N., Senda, T., Kumar, B.V., Thome, J.J.C., Gordon, C.L.,
15 Miron, M., Weiner, J., Connors, T., *et al.* (2018). Human immunology studies using organ
16 donors: Impact of clinical variations on immune parameters in tissues and circulation. *Am J*
17 *Transplant* *18*, 74-88.
- 18
19 Choi, Y.S., Gullicksrud, J.A., Xing, S., Zeng, Z., Shan, Q., Li, F., Love, P.E., Peng, W., Xue,
20 H.H., and Crotty, S. (2015). LEF-1 and TCF-1 orchestrate T(FH) differentiation by regulating
21 differentiation circuits upstream of the transcriptional repressor Bcl6. *Nat Immunol* *16*, 980-990.
- 22
23 Chua, R.L., Lukassen, S., Trump, S., Hennig, B.P., Wendisch, D., Pott, F., Debnath, O.,
24 Thurmann, L., Kurth, F., Volker, M.T., *et al.* (2020). COVID-19 severity correlates with airway
25 epithelium-immune cell interactions identified by single-cell analysis. *Nat Biotechnol* *38*, 970-
26 979.
- 27
28 Cole, S.L., Dunning, J., Kok, W.L., Benam, K.H., Benlahrech, A., Repapi, E., Martinez, F.O.,
29 Drumright, L., Powell, T.J., Bennett, M., *et al.* (2017). M1-like monocytes are a major
30 immunological determinant of severity in previously healthy adults with life-threatening
31 influenza. *JCI Insight* *2*, e91868.
- 32
33 Connors, T.J., Baird, J.S., Yopes, M.C., Zens, K.D., Pethe, K., Ravindranath, T.M., Ho, S.H.,
34 and Farber, D.L. (2018). Developmental Regulation of Effector and Resident Memory T Cell
35 Generation during Pediatric Viral Respiratory Tract Infection. *J Immunol* *201*, 432-439.
- 36
37 Connors, T.J., Ravindranath, T.M., Bickham, K.L., Gordon, C.L., Zhang, F., Levin, B., Baird,
38 J.S., and Farber, D.L. (2016). Airway CD8(+) T Cells Are Associated with Lung Injury during
39 Infant Viral Respiratory Tract Infection. *Am J Respir Cell Mol Biol* *54*, 822-830.

- 1
2 Cummings, M.J., Baldwin, M.R., Abrams, D., Jacobson, S.D., Meyer, B.J., Balough, E.M.,
3 Aaron, J.G., Claassen, J., Rabbani, L.E., Hastie, J., *et al.* (2020). Epidemiology, clinical course,
4 and outcomes of critically ill adults with COVID-19 in New York City: a prospective cohort
5 study. *Lancet* 395, 1763-1770.
- 6
7 Damiani, S., Fiorentino, M., De Palma, A., Foschini, M.P., Lazzarotto, T., Gabrielli, L., Viale,
8 P.L., Attard, L., Riefolo, M., and D'Errico, A. (2021). Pathological post-mortem findings in
9 lungs infected with SARS-CoV-2. *J Pathol* 253, 31-40.
- 10
11 Davies, N.G., Klepac, P., Liu, Y., Prem, K., Jit, M., group, C.C.-w., and Eggo, R.M. (2020).
12 Age-dependent effects in the transmission and control of COVID-19 epidemics. *Nat Med* 26,
13 1205-1211.
- 14
15 De Michele, S., Sun, Y., Yilmaz, M.M., Katsyv, I., Salvatore, M., Dzierba, A.L., Marboe, C.C.,
16 Brodie, D., Patel, N.M., Garcia, C.K., *et al.* (2020). Forty Postmortem Examinations in COVID-
17 19 Patients. *Am J Clin Pathol* 154, 748-760.
- 18
19 Della-Torre, E., Campochiaro, C., Cavalli, G., De Luca, G., Napolitano, A., La Marca, S.,
20 Boffini, N., Da Prat, V., Di Terlizzi, G., Lanzillotta, M., *et al.* (2020). Interleukin-6 blockade
21 with sarilumab in severe COVID-19 pneumonia with systemic hyperinflammation: an open-label
22 cohort study. *Ann Rheum Dis* 79, 1277-1285.
- 23
24 Dogra, P., Rancan, C., Ma, W., Toth, M., Senda, T., Carpenter, D.J., Kubota, M., Matsumoto, R.,
25 Thapa, P., Szabo, P.A., *et al.* (2020). Tissue Determinants of Human NK Cell Development,
26 Function, and Residence. *Cell* 180, 749-763 e713.
- 27
28 Farhadian, S., Glick, L.R., Vogels, C.B.F., Thomas, J., Chiarella, J., Casanovas-Massana, A.,
29 Zhou, J., Odio, C., Vijayakumar, P., Geng, B., *et al.* (2020). Acute encephalopathy with elevated
30 CSF inflammatory markers as the initial presentation of COVID-19. *BMC Neurol* 20, 248.
- 31
32 Furlow, B. (2020). COVACTA trial raises questions about tocilizumab's benefit in COVID-19.
33 *Lancet Rheumatol* 2, e592.
- 34
35 Garibaldi, B.T., Fiksel, J., Muschelli, J., Robinson, M.L., Rouhizadeh, M., Perin, J., Schumock,
36 G., Nagy, P., Gray, J.H., Malapati, H., *et al.* (2021). Patient Trajectories Among Persons
37 Hospitalized for COVID-19 : A Cohort Study. *Ann Intern Med* 174, 33-41.
- 38

- 1 Gartrell, R.D., Marks, D.K., Hart, T.D., Li, G., Davari, D.R., Wu, A., Blake, Z., Lu, Y., Askin,
2 K.N., Monod, A., *et al.* (2018). Quantitative Analysis of Immune Infiltrates in Primary
3 Melanoma. *Cancer Immunol Res* 6, 481-493.
- 4
- 5 Geissmann, F., Jung, S., and Littman, D.R. (2003). Blood monocytes consist of two principal
6 subsets with distinct migratory properties. *Immunity* 19, 71-82.
- 7
- 8 Griffiths, J.A., Richard, A.C., Bach, K., Lun, A.T.L., and Marioni, J.C. (2018). Detection and
9 removal of barcode swapping in single-cell RNA-seq data. *Nature communications* 9, 2667.
- 10
- 11 Grifoni, A., Weiskopf, D., Ramirez, S.I., Mateus, J., Dan, J.M., Moderbacher, C.R., Rawlings,
12 S.A., Sutherland, A., Premkumar, L., Jadi, R.S., *et al.* (2020). Targets of T Cell Responses to
13 SARS-CoV-2 Coronavirus in Humans with COVID-19 Disease and Unexposed Individuals. *Cell*
14 181, 1489-1501 e1415.
- 15
- 16 Hadjadj, J., Yatim, N., Barnabei, L., Corneau, A., Boussier, J., Smith, N., Pere, H., Charbit, B.,
17 Bondet, V., Chenevier-Gobeaux, C., *et al.* (2020). Impaired type I interferon activity and
18 inflammatory responses in severe COVID-19 patients. *Science* 369, 718-724.
- 19
- 20 Hassan, A.O., Kafai, N.M., Dmitriev, I.P., Fox, J.M., Smith, B.K., Harvey, I.B., Chen, R.E.,
21 Winkler, E.S., Wessel, A.W., Case, J.B., *et al.* (2020). A Single-Dose Intranasal ChAd Vaccine
22 Protects Upper and Lower Respiratory Tracts against SARS-CoV-2. *Cell* 183, 169-184 e113.
- 23
- 24 Hendrix, A.Y., and Kheradmand, F. (2017). The Role of Matrix Metalloproteinases in
25 Development, Repair, and Destruction of the Lungs. *Prog Mol Biol Transl Sci* 148, 1-29.
- 26
- 27 Hunter, J.D. (2007). Matplotlib: A 2D graphics environment. *Computing In Science and*
28 *Engineering* 9, 90-95.
- 29
- 30 Jeyanathan, M., Afkhami, S., Smaill, F., Miller, M.S., Lichty, B.D., and Xing, Z. (2020).
31 Immunological considerations for COVID-19 vaccine strategies. *Nat Rev Immunol* 20, 615-632.
- 32
- 33 Jones, A.E., Trzeciak, S., and Kline, J.A. (2009). The Sequential Organ Failure Assessment score
34 for predicting outcome in patients with severe sepsis and evidence of hypoperfusion at the time
35 of emergency department presentation. *Crit Care Med* 37, 1649-1654.
- 36
- 37 Jones, E., Oliphant, T., and Peterson, P. (2001). SciPy: Open source scientific tools for Python.
- 38

- 1 Kapellos, T.S., Bonaguro, L., Gemund, I., Reusch, N., Saglam, A., Hinkley, E.R., and Schultze,
2 J.L. (2019). Human Monocyte Subsets and Phenotypes in Major Chronic Inflammatory Diseases.
3 *Front Immunol* *10*, 2035.
- 4
- 5 Khemani, R.G., Smith, L.S., Zimmerman, J.J., Erickson, S., and Pediatric Acute Lung Injury
6 Consensus Conference, G. (2015). Pediatric acute respiratory distress syndrome: definition,
7 incidence, and epidemiology: proceedings from the Pediatric Acute Lung Injury Consensus
8 Conference. *Pediatr Crit Care Med* *16*, S23-40.
- 9
- 10 Kim, D., Lee, J.Y., Yang, J.S., Kim, J.W., Kim, V.N., and Chang, H. (2020). The Architecture of
11 SARS-CoV-2 Transcriptome. *Cell* *181*, 914-921 e910.
- 12
- 13 Kohlmeier, J.E., and Woodland, D.L. (2009). Immunity to respiratory viruses. *Annu Rev*
14 *Immunol* *27*, 61-82.
- 15
- 16 Korsunsky, I., Millard, N., Fan, J., Slowikowski, K., Zhang, F., Wei, K., Baglaenko, Y., Brenner,
17 M., Loh, P.-r., and Raychaudhuri, S. (2019). Fast, sensitive and accurate integration of single-
18 cell data with Harmony. *Nature Methods* *16*, 1289-1296.
- 19
- 20 Kumar, B.V., Connors, T.J., and Farber, D.L. (2018). Human T Cell Development, Localization,
21 and Function throughout Life. *Immunity* *48*, 202-213.
- 22
- 23 Kumar, B.V., Ma, W., Miron, M., Granot, T., Guyer, R.S., Carpenter, D.J., Senda, T., Sun, X.,
24 Ho, S.H., Lerner, H., *et al.* (2017). Human Tissue-Resident Memory T Cells Are Defined by
25 Core Transcriptional and Functional Signatures in Lymphoid and Mucosal Sites. *Cell Rep* *20*,
26 2921-2934.
- 27
- 28 Kuri-Cervantes, L., Pampera, M.B., Meng, W., Rosenfeld, A.M., Ittner, C.A.G., Weisman, A.R.,
29 Agyekum, R.S., Mathew, D., Baxter, A.E., Vella, L.A., *et al.* (2020). Comprehensive mapping of
30 immune perturbations associated with severe COVID-19. *Sci Immunol* *5*.eabd7114
- 31
- 32 Laing, A.G., Lorenc, A., Del Molino Del Barrio, I., Das, A., Fish, M., Monin, L., Munoz-Ruiz,
33 M., McKenzie, D.R., Hayday, T.S., Francos-Quijorna, I., *et al.* (2020). A dynamic COVID-19
34 immune signature includes associations with poor prognosis. *Nat Med* *26*, 1623-1635.
- 35
- 36 Levine, J.H., Simonds, E.F., Bendall, S.C., Davis, K.L., Amir el, A.D., Tadmor, M.D., Litvin,
37 O., Fienberg, H.G., Jager, A., Zunder, E.R., *et al.* (2015). Data-Driven Phenotypic Dissection of
38 AML Reveals Progenitor-like Cells that Correlate with Prognosis. *Cell* *162*, 184-197.
- 39

- 1 Levitin, H.M., Yuan, J., Cheng, Y.L., Ruiz, F.J.R., Bush, E.C., Bruce, J.N., Canoll, P., Iavarone,
2 A., Lasorella, A., Blei, D.M., *et al.* (2019). De novo Gene Signature Identification from Single-
3 Cell RNA-seq with Hierarchical Poisson Factorization. *Molecular Systems Biology* 15, e8557.
- 4
- 5 Liao, M., Liu, Y., Yuan, J., Wen, Y., Xu, G., Zhao, J., Cheng, L., Li, J., Wang, X., Wang, F., *et*
6 *al.* (2020). Single-cell landscape of bronchoalveolar immune cells in patients with COVID-19.
7 *Nat Med* 26, 842-844.
- 8
- 9 Lin, K.L., Suzuki, Y., Nakano, H., Ramsburg, E., and Gunn, M.D. (2008). CCR2+ monocyte-
10 derived dendritic cells and exudate macrophages produce influenza-induced pulmonary immune
11 pathology and mortality. *J Immunol* 180, 2562-2572.
- 12
- 13 Lin, K.L., Sweeney, S., Kang, B.D., Ramsburg, E., and Gunn, M.D. (2011). CCR2-antagonist
14 prophylaxis reduces pulmonary immune pathology and markedly improves survival during
15 influenza infection. *J Immunol* 186, 508-515.
- 16
- 17 Long, Q.X., Liu, B.Z., Deng, H.J., Wu, G.C., Deng, K., Chen, Y.K., Liao, P., Qiu, J.F., Lin, Y.,
18 Cai, X.F., *et al.* (2020). Antibody responses to SARS-CoV-2 in patients with COVID-19. *Nat*
19 *Med* 26, 845-848.
- 20
- 21 Lucas, C., Wong, P., Klein, J., Castro, T.B.R., Silva, J., Sundaram, M., Ellingson, M.K., Mao, T.,
22 Oh, J.E., Israelow, B., *et al.* (2020). Longitudinal analyses reveal immunological misfiring in
23 severe COVID-19. *Nature* 584, 463-469.
- 24
- 25 Lun, A.T., Bach, K., and Marioni, J.C. (2016). Pooling across cells to normalize single-cell RNA
26 sequencing data with many zero counts. *Genome biology* 17, 75.
- 27
- 28 Lun, A.T., Riesenfeld, S., Andrews, T., Gomes, T., and Marioni, J.C. (2019). EmptyDrops:
29 distinguishing cells from empty droplets in droplet-based single-cell RNA sequencing data.
30 *Genome biology* 20, 1-9.
- 31
- 32 Mathew, D., Giles, J.R., Baxter, A.E., Oldridge, D.A., Greenplate, A.R., Wu, J.E., Alanio, C.,
33 Kuri-Cervantes, L., Pampera, M.B., D'Andrea, K., *et al.* (2020). Deep immune profiling of
34 COVID-19 patients reveals distinct immunotypes with therapeutic implications. *Science* 369.
35 eabc8511
- 36
- 37 Matics, T.J., and Sanchez-Pinto, L.N. (2017). Adaptation and Validation of a Pediatric
38 Sequential Organ Failure Assessment Score and Evaluation of the Sepsis-3 Definitions in
39 Critically Ill Children. *JAMA Pediatr* 171, e172352.

- 1
2 McInnes, L., Healy, J., Saul, N., and Grossberger, L. (2018). UMAP: Uniform Manifold
3 Approximation and Projection. *J Open Source Software* 3, 861.
- 4
5 Melsted, P., Boeshaghi, A.S., Gao, F., Beltrame, E., Lu, L., Hjorleifsson, K.E., Gehring, J., and
6 Pachter, L. (2019a). Modular and efficient pre-processing of single-cell RNA-seq. *bioRxiv*,
7 673285.
- 8
9 Melsted, P., Ntranos, V., and Pachter, L. (2019b). The barcode, UMI, set format and BUStools.
10 *Bioinformatics (Oxford, England)* 35, 4472-4473.
- 11
12 Morrell, E.D., Bhatraju, P.K., Mikacenic, C.R., Radella, F., 2nd, Manicone, A.M., Stapleton,
13 R.D., Wurfel, M.M., and Gharib, S.A. (2019). Alveolar Macrophage Transcriptional Programs
14 Are Associated with Outcomes in Acute Respiratory Distress Syndrome. *Am J Respir Crit Care*
15 *Med* 200, 732-741.
- 16
17 Ni, L., Ye, F., Cheng, M.L., Feng, Y., Deng, Y.Q., Zhao, H., Wei, P., Ge, J., Gou, M., Li, X., *et*
18 *al.* (2020). Detection of SARS-CoV-2-Specific Humoral and Cellular Immunity in COVID-19
19 Convalescent Individuals. *Immunity* 52, 971-977 e973.
- 20
21 Oshansky, C.M., Gartland, A.J., Wong, S.S., Jeevan, T., Wang, D., Roddam, P.L., Caniza, M.A.,
22 Hertz, T., Devincenzo, J.P., Webby, R.J., *et al.* (2014). Mucosal immune responses predict
23 clinical outcomes during influenza infection independently of age and viral load. *Am J Respir*
24 *Crit Care Med* 189, 449-462.
- 25
26 Paik, D.H., and Farber, D.L. (2021). Influenza infection fortifies local lymph nodes to promote
27 lung-resident heterosubtypic immunity. *J Exp Med* 218, e20200218.
- 28
29 Pedregosa, F., Varoquaux, G., Gramfort, A., Michel, V., Thirion, B., Grisel, O., Blondel, M.,
30 Prettenhofer, P., Weiss, R., Dubourg, V., *et al.* (2011). Scikit-learn: Machine Learning in Python.
31 *J Mach Learn Res* 12, 2825-2830.
- 32
33 Ranieri, V.M., Rubenfeld, G.D., Thompson, B.T., Ferguson, N.D., Caldwell, E., Fan, E.,
34 Camporota, L., and Slutsky, A.S. (2012). Acute respiratory distress syndrome: the Berlin
35 Definition. *JAMA* 307, 2526-2533.
- 36
37 Rydzynski Moderbacher, C., Ramirez, S.I., Dan, J.M., Grifoni, A., Hastie, K.M., Weiskopf, D.,
38 Belanger, S., Abbott, R.K., Kim, C., Choi, J., *et al.* (2020). Antigen-Specific Adaptive Immunity
39 to SARS-CoV-2 in Acute COVID-19 and Associations with Age and Disease Severity. *Cell* 183,
40 996-1012 e1019.

- 1
2 Sathaliyawala, T., Kubota, M., Yudanin, N., Turner, D., Camp, P., Thome, J.J., Bickham, K.L.,
3 Lerner, H., Goldstein, M., Sykes, M., *et al.* (2013). Distribution and compartmentalization of
4 human circulating and tissue-resident memory T cell subsets. *Immunity* 38, 187-197.
- 5
6 Schulte-Schrepping, J., Reusch, N., Paclik, D., Bassler, K., Schlickeiser, S., Zhang, B., Kramer,
7 B., Krammer, T., Brumhard, S., Bonaguro, L., *et al.* (2020). Severe COVID-19 Is Marked by a
8 Dysregulated Myeloid Cell Compartment. *Cell* 182, 1419-1440 e1423.
- 9
10 Schultze, J.L., Mass, E., and Schlitzer, A. (2019). Emerging Principles in Myelopoiesis at
11 Homeostasis and during Infection and Inflammation. *Immunity* 50, 288-301.
- 12
13 Shekhar, K., Lapan, S.W., Whitney, I.E., Tran, N.M., Macosko, E.Z., Kowalczyk, M., Adiconis,
14 X., Levin, J.Z., Nemesh, J., Goldman, M., *et al.* (2016). Comprehensive Classification of Retinal
15 Bipolar Neurons by Single-Cell Transcriptomics. *Cell* 166, 1308-1323 e1330.
- 16
17 Shi, C., Jia, T., Mendez-Ferrer, S., Hohl, T.M., Serbina, N.V., Lipuma, L., Leiner, I., Li, M.O.,
18 Frenette, P.S., and Pamer, E.G. (2011). Bone marrow mesenchymal stem and progenitor cells
19 induce monocyte emigration in response to circulating toll-like receptor ligands. *Immunity* 34,
20 590-601.
- 21
22 Silvin, A., Chapuis, N., Dunsmore, G., Goubet, A.G., Dubuisson, A., Derosa, L., Almire, C.,
23 Henon, C., Kosmider, O., Droin, N., *et al.* (2020). Elevated Calprotectin and Abnormal Myeloid
24 Cell Subsets Discriminate Severe from Mild COVID-19. *Cell* 182, 1401-1418 e1418.
- 25
26 Singer, M., Deutschman, C.S., Seymour, C.W., Shankar-Hari, M., Annane, D., Bauer, M.,
27 Bellomo, R., Bernard, G.R., Chiche, J.D., Cooper-Smith, C.M., *et al.* (2016). The Third
28 International Consensus Definitions for Sepsis and Septic Shock (Sepsis-3). *JAMA* 315, 801-
29 810.
- 30
31 Snyder, M.E., Finlayson, M.O., Connors, T.J., Dogra, P., Senda, T., Bush, E., Carpenter, D.,
32 Marboe, C., Benvenuto, L., Shah, L., *et al.* (2019). Generation and persistence of human tissue-
33 resident memory T cells in lung transplantation. *Sci Immunol* 4, eaav5581.
- 34
35 Szabo, P.A., Levitin, H.M., Miron, M., Snyder, M.E., Senda, T., Yuan, J., Cheng, Y.L., Bush,
36 E.C., Dogra, P., Thapa, P., *et al.* (2019). Single-cell transcriptomics of human T cells reveals
37 tissue and activation signatures in health and disease. *Nat Commun* 10, 4706.
- 38

- 1 Takahashi, T., Ellingson, M.K., Wong, P., Israelow, B., Lucas, C., Klein, J., Silva, J., Mao, T.,
2 Oh, J.E., Tokuyama, M., *et al.* (2020). Sex differences in immune responses that underlie
3 COVID-19 disease outcomes. *Nature* 588, 315-320.
- 4
- 5 Teijaro, J.R., Turner, D., Pham, Q., Wherry, E.J., Lefrancois, L., and Farber, D.L. (2011a).
6 Cutting edge: tissue-retentive lung memory CD4 T cells mediate optimal protection to
7 respiratory virus infection. *J Immunol* 187, 5510-5514.
- 8
- 9 Teijaro, J.R., Walsh, K.B., Cahalan, S., Fremgen, D.M., Roberts, E., Scott, F., Martinborough,
10 E., Peach, R., Oldstone, M.B., and Rosen, H. (2011b). Endothelial cells are central orchestrators
11 of cytokine amplification during influenza virus infection. *Cell* 146, 980-991.
- 12
- 13 Thieme, C.J., Anft, M., Paniskaki, K., Blazquez-Navarro, A., Doevelaar, A., Seibert, F.S.,
14 Hoelzer, B., Konik, M.J., Brenner, T., Tempfer, C., *et al.* (2020). Robust T cell response towards
15 spike, membrane, and nucleocapsid SARS-CoV-2 proteins is not associated with recovery in
16 critical COVID-19 patients. *Cell Rep Med*, 100092.
- 17
- 18 Thome, J.J., Yudanin, N., Ohmura, Y., Kubota, M., Grinshpun, B., Sathaliyawala, T., Kato, T.,
19 Lerner, H., Shen, Y., and Farber, D.L. (2014). Spatial map of human T cell compartmentalization
20 and maintenance over decades of life. *Cell* 159, 814-828.
- 21
- 22 Turner, D.L., Bickham, K.L., Thome, J.J., Kim, C.Y., D'Ovidio, F., Wherry, E.J., and Farber,
23 D.L. (2014). Lung niches for the generation and maintenance of tissue-resident memory T cells.
24 *Mucosal Immunol* 7, 501-510.
- 25
- 26 Turner, D.L., and Farber, D.L. (2014). Mucosal resident memory CD4 T cells in protection and
27 immunopathology. *Front Immunol* 5, 331.
- 28
- 29 van der Walt, S., Colbert, S.C., and Varoquaux, G. (2011). The NumPy Array: A Structure for
30 Efficient Numerical Computation. *Computing in Science & Engineering* 13, 22-30.
- 31
- 32 Vasilevskis, E.E., Pandharipande, P.P., Graves, A.J., Shintani, A., Tsuruta, R., Ely, E.W., and
33 Girard, T.D. (2016). Validity of a Modified Sequential Organ Failure Assessment Score Using
34 the Richmond Agitation-Sedation Scale. *Crit Care Med* 44, 138-146.
- 35
- 36 Venet, F., Demaret, J., Gossez, M., and Monneret, G. (2020). Myeloid cells in sepsis-acquired
37 immunodeficiency. *Ann N Y Acad Sci*. doi: 10.1111/nyas.14333. Online ahead of print
- 38

- 1 Veras, F.P., Pontelli, M.C., Silva, C.M., Toller-Kawahisa, J.E., de Lima, M., Nascimento, D.C.,
2 Schneider, A.H., Caetite, D., Tavares, L.A., Paiva, I.M., *et al.* (2020). SARS-CoV-2-triggered
3 neutrophil extracellular traps mediate COVID-19 pathology. *J Exp Med* 217, e29291129.
- 4
- 5 Vincent, J.L., de Mendonca, A., Cantraine, F., Moreno, R., Takala, J., Suter, P.M., Sprung, C.L.,
6 Colardyn, F., and Blecher, S. (1998). Use of the SOFA score to assess the incidence of organ
7 dysfunction/failure in intensive care units: results of a multicenter, prospective study. Working
8 group on "sepsis-related problems" of the European Society of Intensive Care Medicine. *Crit*
9 *Care Med* 26, 1793-1800.
- 10
- 11 Weisberg, S.P., Carpenter, D.J., Chait, M., Dogra, P., Gartrell-Corrado, R.D., Chen, A.X.,
12 Campbell, S., Liu, W., Saraf, P., Snyder, M.E., *et al.* (2019). Tissue-Resident Memory T Cells
13 Mediate Immune Homeostasis in the Human Pancreas through the PD-1/PD-L1 Pathway. *Cell*
14 *Rep* 29, 3916-3932 e3915.
- 15
- 16 Weisberg, S.P., Connors, T.J., Zhu, Y., Baldwin, M.R., Lin, W.H., Wontakal, S., Szabo, P.A.,
17 Wells, S.B., Dogra, P., Gray, J., *et al.* (2021). Distinct antibody responses to SARS-CoV-2 in
18 children and adults across the COVID-19 clinical spectrum. *Nat Immunol* 22, 25-31.
- 19
- 20 Weiskopf, D., Schmitz, K.S., Raadsen, M.P., Grifoni, A., Okba, N.M.A., Endeman, H., van den
21 Akker, J.P.C., Molenkamp, R., Koopmans, M.P.G., van Gorp, E.C.M., *et al.* (2020). Phenotype
22 and kinetics of SARS-CoV-2-specific T cells in COVID-19 patients with acute respiratory
23 distress syndrome. *Sci Immunol* 5, eabd2071.
- 24
- 25 Wu, T., Hu, Y., Lee, Y.T., Bouchard, K.R., Benechet, A., Khanna, K., and Cauley, L.S. (2014).
26 Lung-resident memory CD8 T cells (TRM) are indispensable for optimal cross-protection
27 against pulmonary virus infection. *J Leukoc Biol* 95, 215-224.
- 28
- 29 Wu, Z., and McGoogan, J.M. (2020). Characteristics of and Important Lessons From the
30 Coronavirus Disease 2019 (COVID-19) Outbreak in China: Summary of a Report of 72314
31 Cases From the Chinese Center for Disease Control and Prevention. *JAMA* 323, 1239-1242.
- 32
- 33 Yoo, J.K., Kim, T.S., Hufford, M.M., and Braciale, T.J. (2013). Viral infection of the lung: host
34 response and sequelae. *J Allergy Clin Immunol* 132, 1263-1276; quiz 1277.
- 35
- 36 Zhao, J., Zhao, J., Mangalam, A.K., Channappanavar, R., Fett, C., Meyerholz, D.K.,
37 Agnihothram, S., Baric, R.S., David, C.S., and Perlman, S. (2016). Airway Memory CD4(+) T
38 Cells Mediate Protective Immunity against Emerging Respiratory Coronaviruses. *Immunity* 44,
39 1379-1391.
- 40

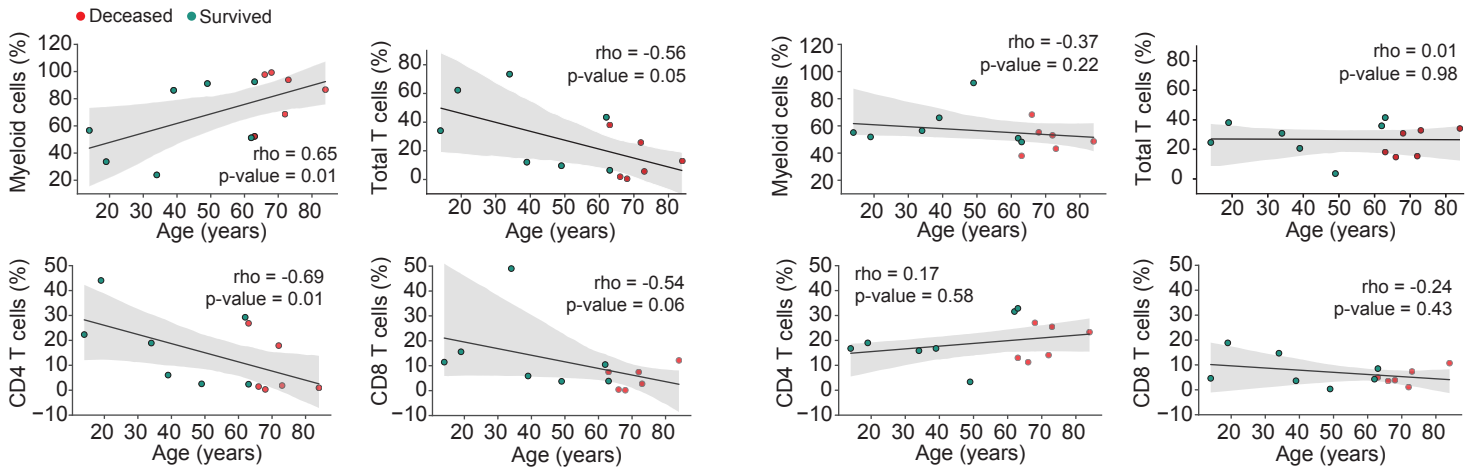
Highlights:

- Airways show localized immune responses correlating to age and outcome in COVID-19
- Airway T cells are activated and resident while myeloid cells are hyperinflammatory
- Aberrant CD163^{hi} and HLA-DR^{lo} monocytes predominate in COVID-19 blood
- Monocytes infiltrate airways and lung alveoli potentially through a CCL2-CCR2 axis

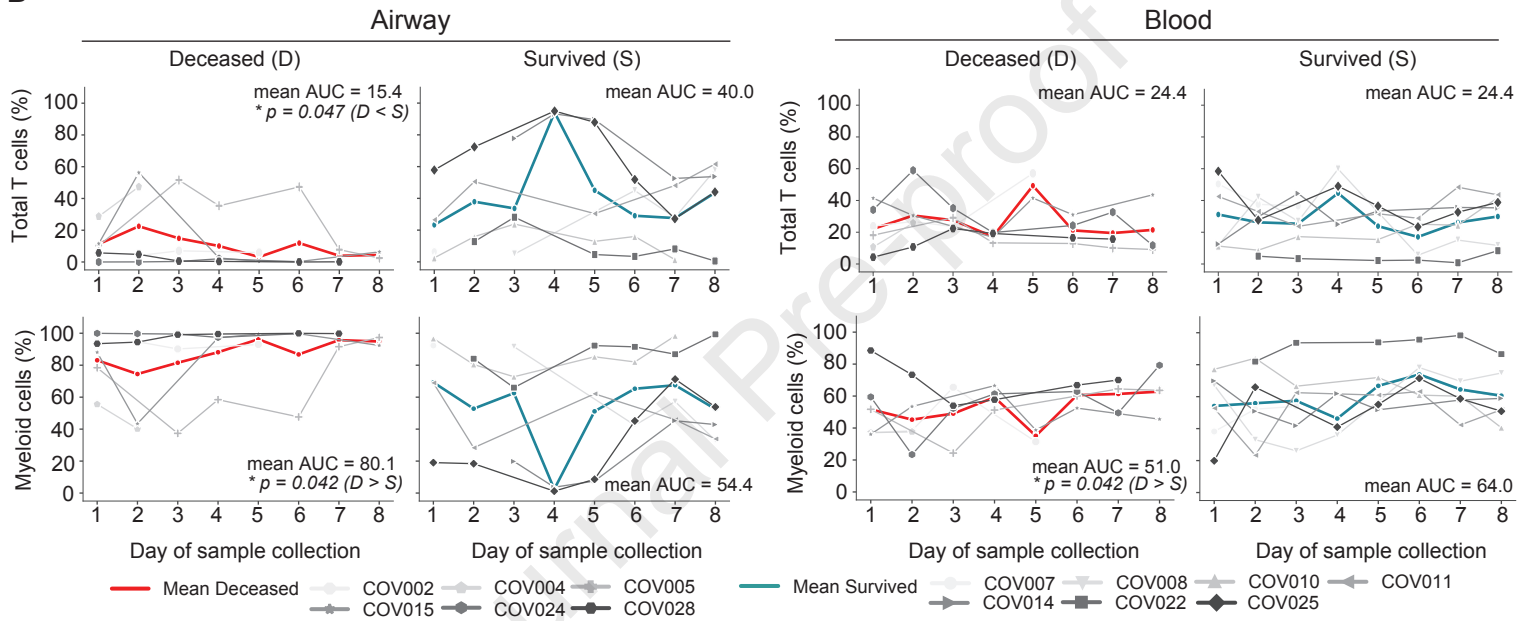
eTOC Blurb (50 words)

Through longitudinal profiling of paired airway and blood from patients with severe COVID-19, Szabo et al. reveal airway immune responses that correlate with age and outcome. They further identify coordinate roles for T and myeloid cells in the respiratory tract and circulation in perpetuating lung pathology and disease pathogenesis.

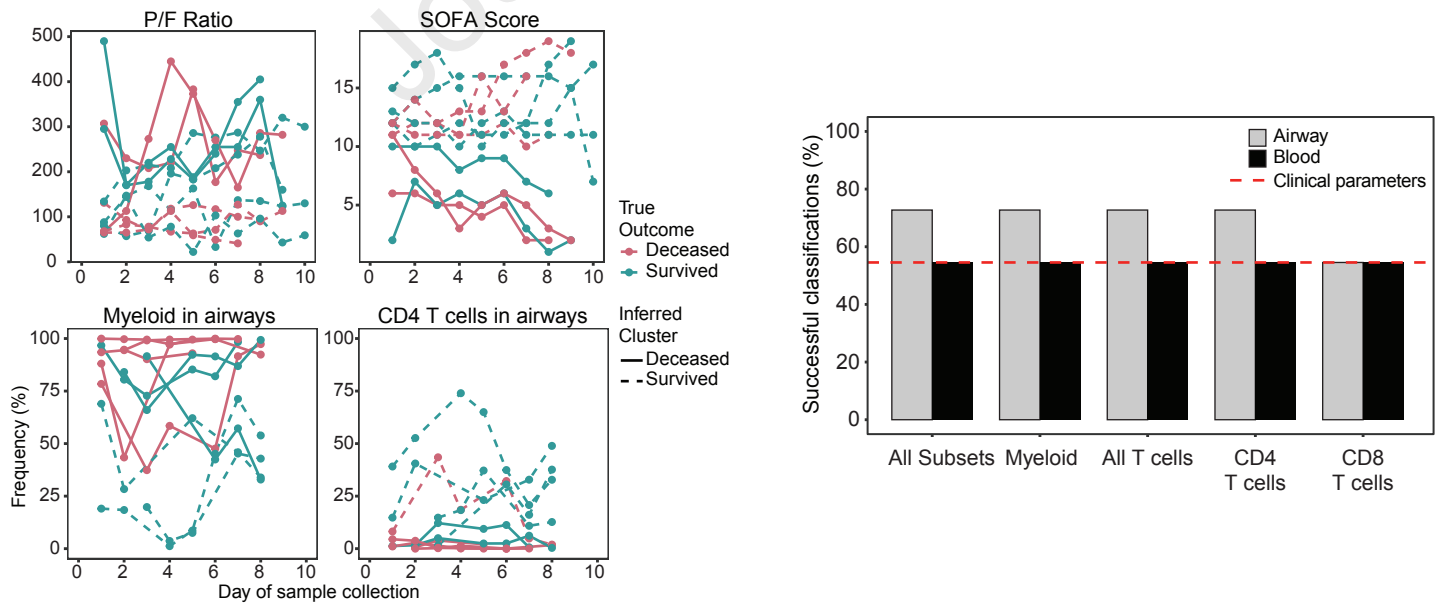
A



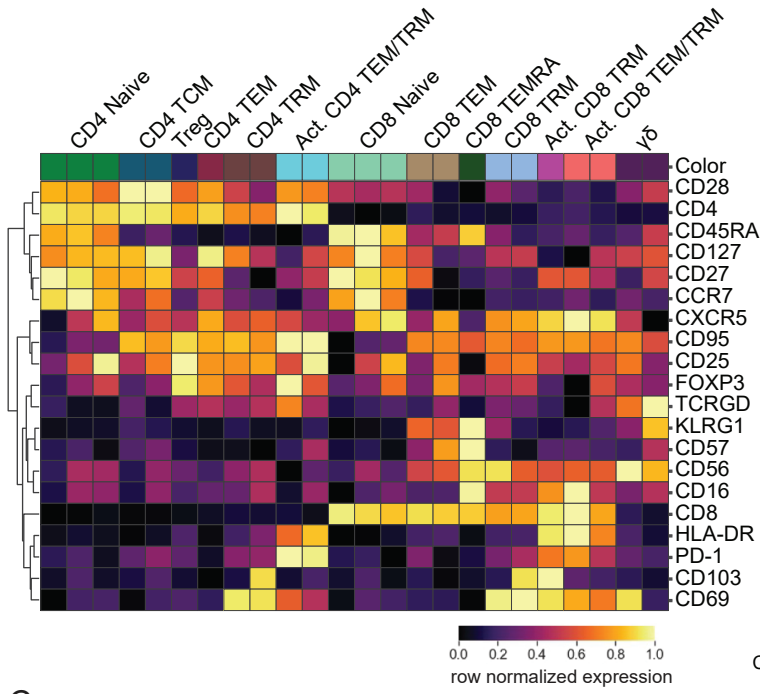
B



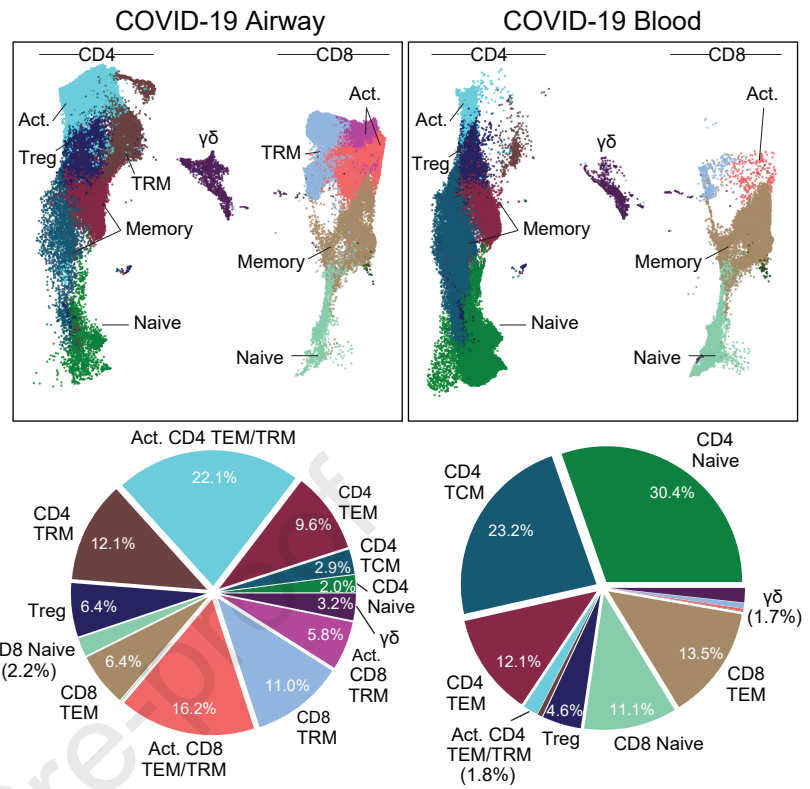
C



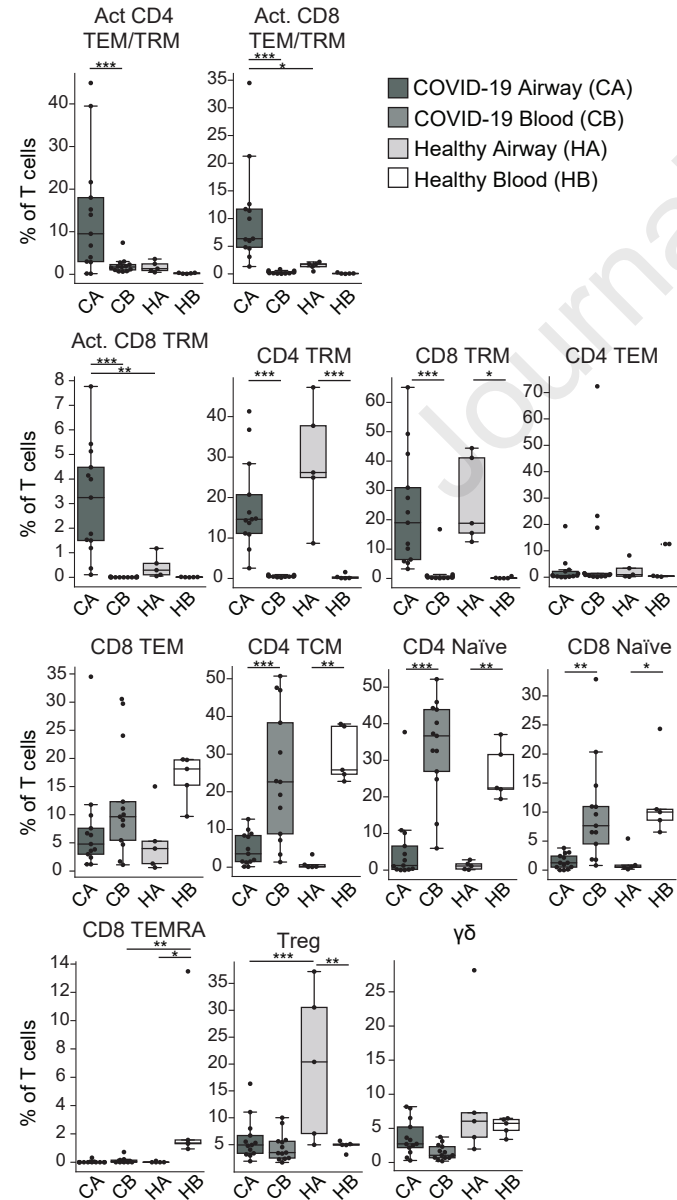
A



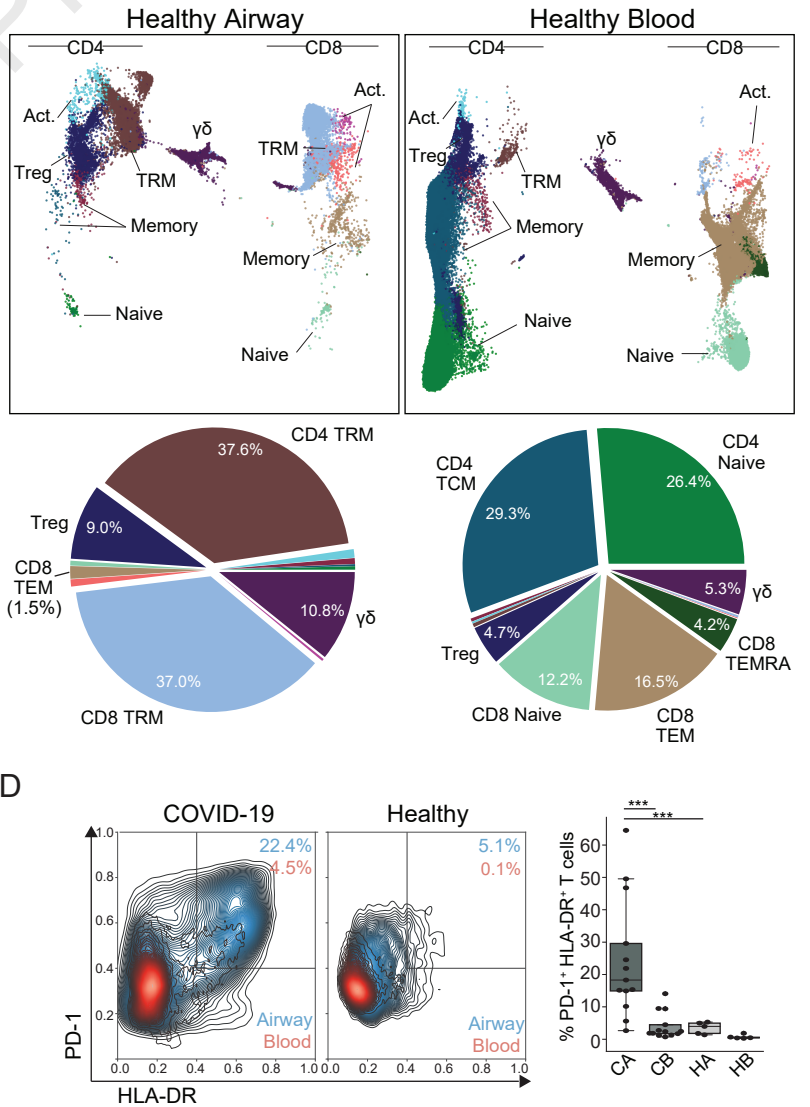
B



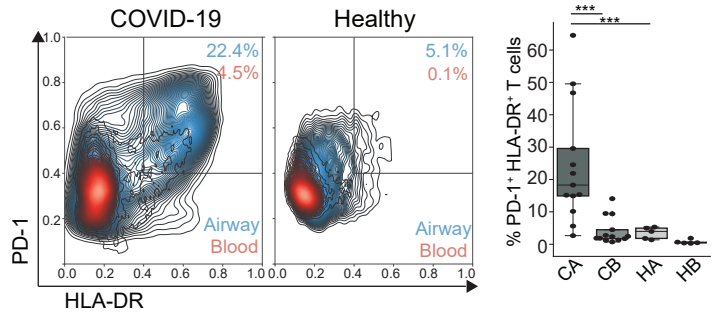
C



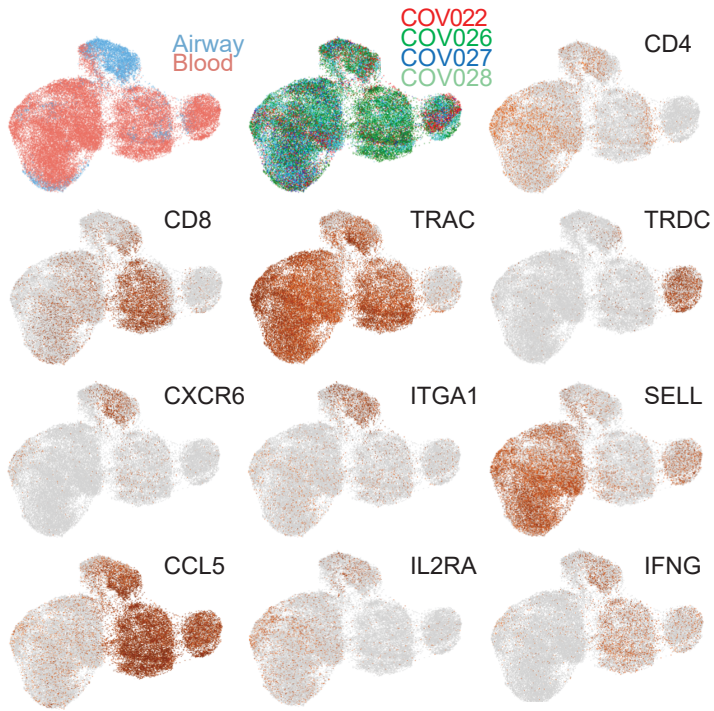
D



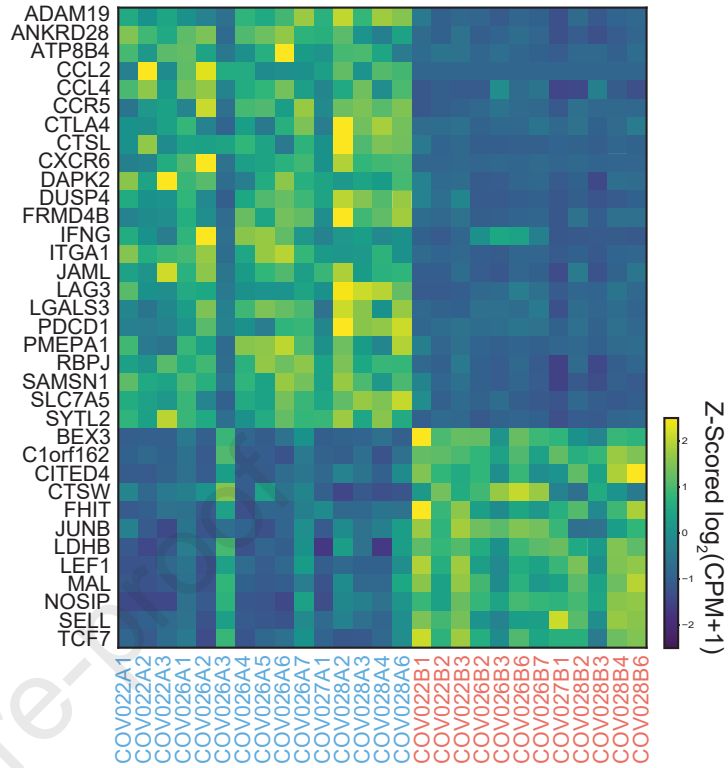
D



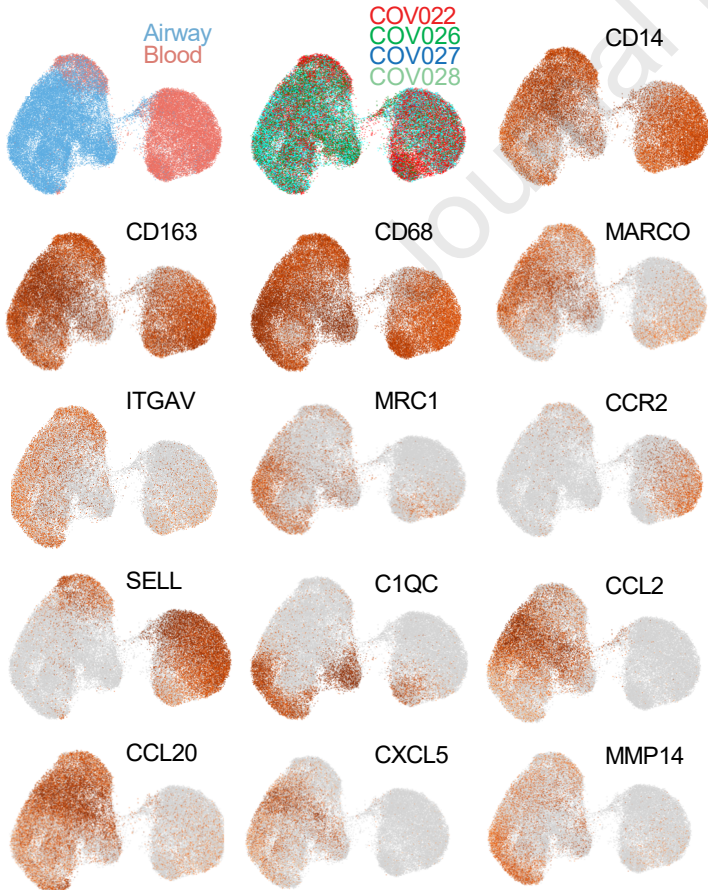
A



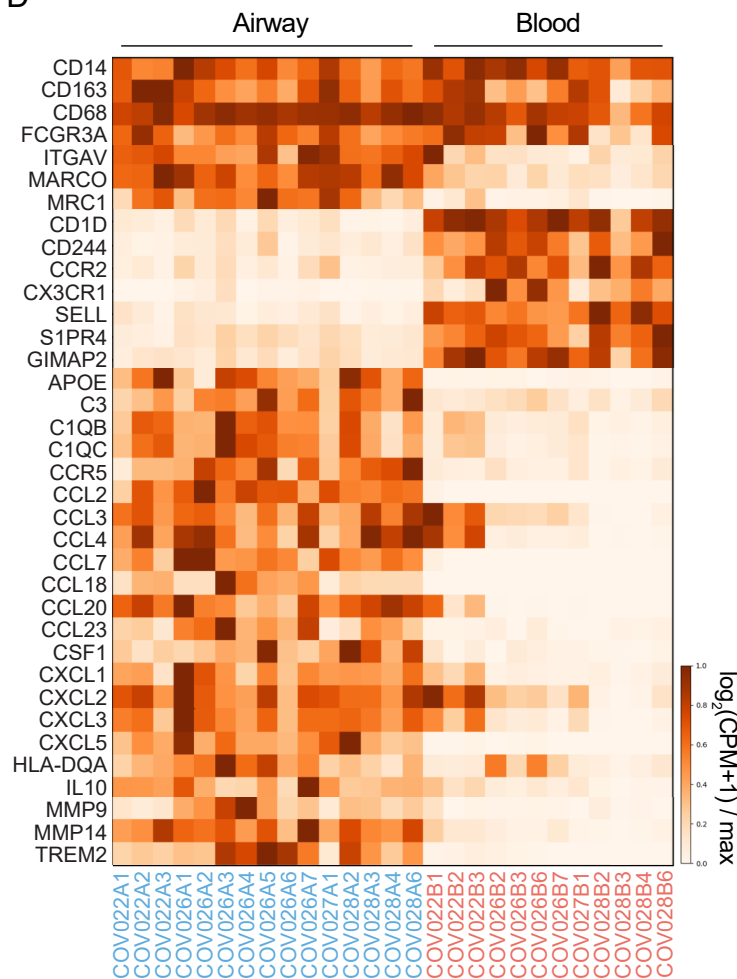
Airway Blood



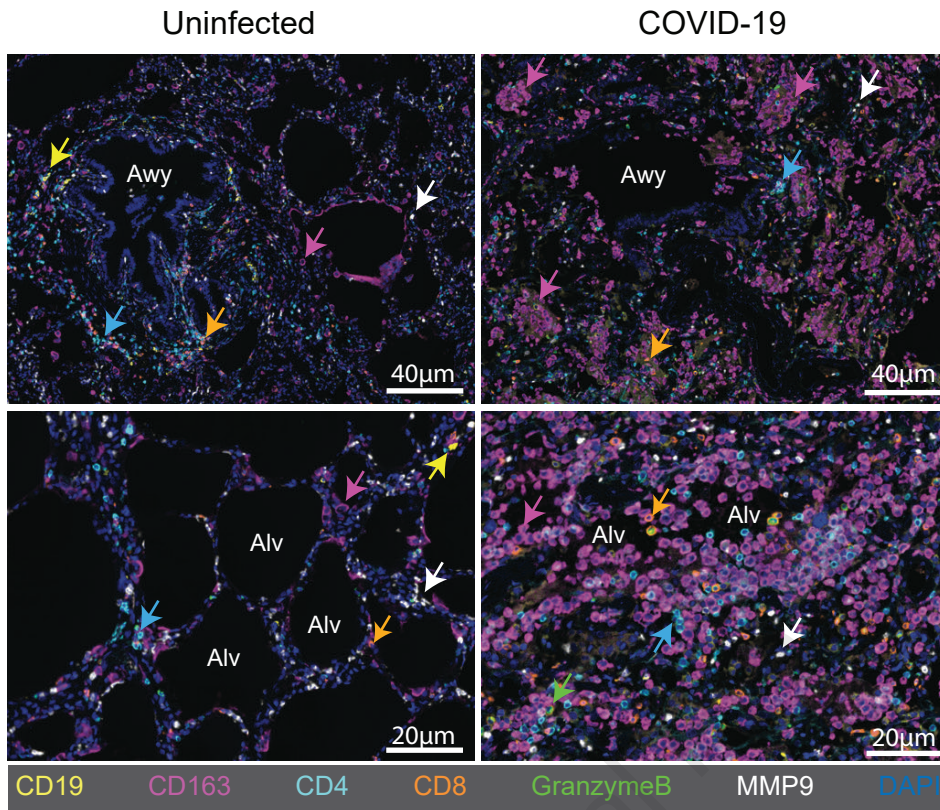
C



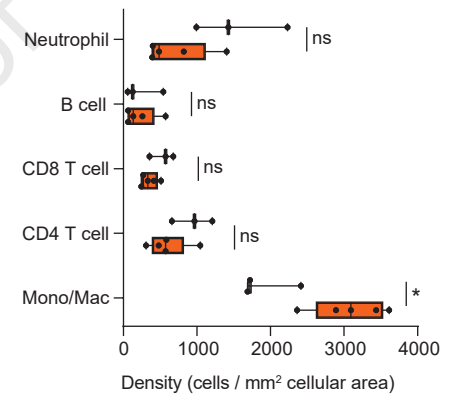
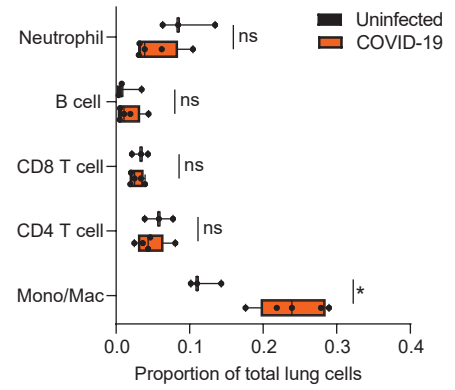
D



A



B



C

